

Istraživanje osjetljivosti stanične linije SU-DHL-5 s mutacijama gena KLHL6 na lijekove

Tandarić, Luka

Master's thesis / Diplomski rad

2019

Degree Grantor / Ustanova koja je dodijelila akademski / stručni stupanj: **University of Zagreb, Faculty of Science / Sveučilište u Zagrebu, Prirodoslovno-matematički fakultet**

Permanent link / Trajna poveznica: <https://um.nsk.hr/um:nbn:hr:217:503841>

Rights / Prava: [In copyright](#) / [Zaštićeno autorskim pravom.](#)

Download date / Datum preuzimanja: **2025-02-12**



Repository / Repozitorij:

[Repository of the Faculty of Science - University of Zagreb](#)



University of Zagreb
Faculty of Science
Department of Biology

Luka Tandarić

Analysis of Drug Sensitivity Effects of *KLHL6* Mutations in the SU-DHL-5 Cell Line

Graduation thesis

Zagreb, 2019

This thesis has been created in the laboratory of the Lymphoma Biology and Survival research group of the Applied Tumor Genomics research program of the Faculty of Medicine of the University of Helsinki, under the supervision of prof. Sirpa Leppä, MD PhD. This thesis has been submitted for evaluation to the Department of Biology at the Faculty of Science of the University of Zagreb with the aim of obtaining the title of Master of Science in Molecular Biology.

ACKNOWLEDGEMENTS

I would like to express my sincerest gratitude to prof. Sirpa Leppä, MD PhD, without whose hard work, generosity and trust I would not have been able to accomplish my academic goals by doing what I love and researching a field of my highest interest.

Thank you to BM Leo Meriranta, who graciously provided me with the subject matter to base my master's thesis on, offered me advice, and always answered my endless questions during my work in the lab.

Thank you to doc. PhD Marko Hyytiäinen, who provided professional guidance on the laboratory techniques I used, and counseled me on the writing of this thesis along with BM Leo Meriranta.

Thank you to the rest of the Lymphoma Biology and Survival group for your unconditional support.

Thank you to Jani Saarela, Swapnil Potdar, and Philipp Ianevski of the DSRT team of the High Throughput Biomedicine Unit of FIMM for performing the DSRT and providing the drug response curves of the verification experiments.

Thank you to the faculty of the Erasmus Plus student mobility programme, whose encouragement and financial support of students who wish to study abroad made my stay in Finland possible.

A heartfelt thank you to Assoc. Prof. dr. sc. Petra Korać for directing my interests towards cancer research, for providing me with quality education, both theoretical and practical, and lastly for helping me achieve the title of Master of Science in Molecular Biology by supervising both the writing of my application to the Lymphoma Biology and Survival group and this master's thesis.

Finally, thank you to all my family and friends who provided me with support and comfort throughout my life, with special thanks to my sister, mother, and grandmother, and Tomislav, Nikolina, Matej, Antonia, Leda, Iva and Ana.

BASIC DOCUMENTATION CARD

University of Zagreb
Faculty of Science
Division of Biology

Graduation Thesis

Analysis of Drug Sensitivity Effects of *KLHL6* Mutations in the SU-DHL-5 Cell Line

Luka Tandarić

Roosevelt Square 6, 10000 Zagreb, Croatia

Diffuse large B-cell lymphoma (DLBCL) is the most common non-Hodgkin lymphoma worldwide. Several types of DLBCL are currently recognized by the World Health Organization, with the most common type being DLBCL, NOS (not otherwise specified). Kelch-like protein 6 (*KLHL6*), a protein involved in B-lymphocyte maturation, has been found to carry mutations in about 10 % of DLBCL, NOS cases. The goals of this study were the characterization of the effects these mutations have on drug response, and consequent elucidation of cellular pathways *KLHL6* is involved in. SU-DHL-5 cells, a GCB-type DLBCL, NOS model, were lentivirally-transduced with mutant and wild-type *KLHL6* constructs to express the proteins. A panel of 528 drugs was used in order to comprehensively detect effects of the most common mutations on drug response, and differences in the viability between SU-DHL-5 cells expressing wild-type and mutant *KLHL6* were determined. Preliminary drug screen results suggested that some mutations modify the response to certain groups of drugs affecting the same cellular pathway, e.g. the PI3K/Akt pathway. However, verification experiments were unable to reproduce the results, and no significant effects of *KLHL6* mutations on drug response were observed, which puts the significance of the explored *KLHL6* mutations in DLBCL into question.

(78 pages, 15 figures, 8 tables, 123 references, original in English)

Thesis deposited in the Central Biological Library

Keywords: lentiviral transduction, DSRT, kelch-like protein 6, non-Hodgkin's lymphoma

Supervisor: Dr. Sirpa Leppä, MD, Prof. PhD Cosupervisor: Dr. Petra Korać, Assoc. Prof.

Reviewers: Dr. Petra Korać, Assoc. Prof.

Dr. Antun Alegro, Assoc. Prof.

Dr. Sofia Ana Blažević, Asst. Prof.

Thesis accepted: September 18th, 2019

TEMELJNA DOKUMENTACIJSKA KARTICA

Sveučilište u Zagrebu

Prirodoslovno-matematički fakultet

Biološki Odsjek

Diplomski Rad

Istraživanje osjetljivosti stanične linije SU-DHL-5 s mutacijama gena *KLHL6* na lijekove

Luka Tandarić

Rooseveltov trg 6, 10000 Zagreb, Hrvatska

Difuzni velikostanični B-limfom (DLBCL, od eng. *diffuse large B-cell lymphoma*) najučestaliji je oblik ne-Hodgkinovog limfoma. Svjetska zdravstvena organizacija trenutno definira više tipova DLBCL-a, najučestaliji od kojih je DLBCL, neodređeni tip (NOS, od eng. *not otherwise specified*). Protein 6 sličan proteinu Kelch (*KLHL6*, od eng. *kelch-like protein 6*) uključen je u sazrijevanje B-limfocita i u otprilike 10% slučajeva DLBCL, NOS-a pronađena je njegova mutacija. Ciljevi ovog istraživanja bili su karakterizacija učinaka najučestalijih mutacija *KLHL6* na odgovor na lijekove i posljedično otkrivanje staničnih putova u kojima *KLHL6* sudjeluje. Stanice SU-DHL-5 (od eng. *Stanford University diffuse histiocytic lymphoma 5*), model DLBCL, NOS-a tipa GCB (od eng. *germinal center B-cell-like*), lentivirusno su transducirane ekspresijskim konstruktima koji kodiraju proteine *KLHL6* divljeg i mutiranog tipa. Radi sveobuhvatnog razotkrivanja učinaka najučestalijih mutacija na odgovor na lijekove, upotrebljen je panel od 528 lijekova, nakon čega su određene razlike u vijabilnosti između stanica SU-DHL-5 koje ekspimiraju nemutirane i mutirane gene za protein *KLHL6*. Početni rezultati probira sugerirali su da neke ispitane mutacije mijenjaju odgovor na određene skupine lijekova koji djeluju na isti stanični put, npr. na put PI3K/Akt. Međutim, nakon pokušaja potvrde rezultata, značajni utjecaji mutacija na odgovor na lijekove nisu uočeni, što dovodi postojanje učinaka ispitivanih mutacija *KLHL6* u DLBCL-u u pitanje.

(78 stranica, 15 slika, 8 tablica, 123 literaturna navoda, original na engleskom jeziku)

Rad je pohranjen u Središnjoj biološkoj knjižnici

Ključne riječi: transdukcija lentivirusima, DSRT, kelch-u sličan protein 6, neHodgkinov limfom

Voditelj: Dr. sc. med. Sirpa Leppä, prof.

Suvoditelj: Dr. sc Petra Korać, izv. prof.

Ocjenitelji: Dr. sc Petra Korać, izv. prof.

Dr. sc. Antun Alegro, izv. prof.

Dr. sc. Sofia Ana Blažević, doc.

Rad prihvaćen: 18. rujna 2019.

ABBREVIATIONS

ABC - activated B-cell-like

ATCC - American Type Culture Collection

BACK - BTB and C-terminal kelch

BCR - B-cell receptor

BTB - broad-complex, tramtrack and bric-a-brac

BTK - Bruton tyrosine kinase

COO - cell of origin

CTG - CellTiter-Glo®

dDSS - differential drug sensitivity score

DLBCL - diffuse large B-cell lymphoma

DMSO - dimethyl sulfoxide

DSMZ - die Deutsche Sammlung von Mikroorganismen und Zellkulturen (eng. *the German Collection of Microorganisms and Cell Cultures*)

DSRT - drug sensitivity and resistance testing

DSS - drug sensitivity score

EmGFP - emerald green fluorescent protein

FBS - fetal bovine serum

FIMM - Institute for Molecular Medicine Finland

GCB - germinal center B-cell-like

GEP - gene expression profiling

IC₅₀ - half-maximal inhibitory concentration

ICLC - Interlab Cell Line Collection

IPI - international prognostic index

ITAM - immunoreceptor tyrosine-based activation motif

JCRB - Japanese Cancer Research Resources Bank

KLHL - kelch-like

KLHL6 - kelch-like protein 6

NHL - non-Hodgkin's lymphoma

NCCN - National Comprehensive Cancer Network

OS - overall survival

R-CHOP - rituximab, cyclophosphamide, doxorubicin, vincristine, and prednisone

RPMI 1640 - Roswell Park Memorial Institute (medium) 1640

RT - room temperature

SU-DHL - Stanford University - Diffuse Histiocytic Lymphoma

TBST - tris-buffered saline / Tween 20

TIR domain - toll/interleukin-1 receptor (TIR) homology domain

WHO - World Health Organization

Contents

1. INTRODUCTION	1
1.1 Diffuse Large B-Cell Lymphoma.....	1
1.1.1 Types of DLBCL	1
1.1.2 Staging and Prediction of Clinical Outcome	7
1.1.3 Signaling Pathways Commonly Altered in GCB-DLBCL.....	9
1.1.4 Signaling Pathways Commonly Altered in ABC-DLBCL.....	11
1.1.5 Courses of Treatment.....	13
1.2 The BTB-kelch Protein Family and Kelch-Repeat Superfamily.....	13
1.2.1 The Structure of Kelch-Repeat Proteins	13
1.2.2 The Functions of Kelch-Repeat Proteins	16
1.3 Kelch-Like Protein 6	16
1.3.1 Structure of KLHL6.....	16
1.3.2 Proposed Roles of KLHL6 in the Cell.....	17
1.3.3 KLHL6 in Malignancies	17
1.4 Drug Sensitivity Score.....	18
1.4.1 The Mathematics Behind the Drug Sensitivity Score.....	18
2. AIM OF THE STUDY	21
3. MATERIALS AND METHODS	22
3.1 Materials	22
3.1.1 The SU-DHL-4 Cell Line	22
3.1.2 The SU-DHL-5 Cell Lines.....	22
3.2 Methods	23
3.2.1 Maintenance of SU-DHL-5 Cell Cultures	23
3.2.2 Extraction of DNA from Cells for Cell Line Authentication	24
3.2.3 Extraction of Total Cytosolic Protein from Cells	25
3.2.4 Protein Quantification.....	25
3.2.5 Western Blotting	26
3.2.6 Mycoplasma Infection Assay	27
3.2.7 Cell Proliferation Assay.....	28
3.2.8 Drug Sensitivity and Resistance Testing	28
3.2.9 Verification of DSRT Results.....	30
4. RESULTS	32

4.1 Preparation of Cells for Drug Screening	32
4.1.1 Cell Line Authentication.....	32
4.1.2 Cytoplasmic Protein Concentrations of Cell Lines	34
4.1.3 Confirmation of Expression Levels of KLHL6 Variants in SU-DHL-5 Cells	35
4.1.4 Detection of Mycoplasma Infection of Cell Cultures	38
4.1.5 Relative Proliferation Rates of Transduced Cells.....	39
4.2 Drug Sensitivity and Resistance Testing	40
4.3 Verification of DSRT Results	45
5. DISCUSSION	51
5.1 Studied KLHL6 Mutations Might Not Affect Drug Response	51
5.2 Possible Influences on the Outcome of the Study	53
5.3 Future Prospects	54
6. CONCLUSION	55
7. REFERENCES.....	56
8. CURRICULUM VITAE.....	69

1. INTRODUCTION

1.1 Diffuse Large B-Cell Lymphoma

Diffuse large B-cell lymphoma (DLBCL) is the most common type of non-Hodgkin lymphoma (NHL), constituting roughly 30-40 % of cases worldwide, with a higher prevalence in developing regions. While it can be diagnosed in people within any age group, DLBCL usually presents itself in the elderly, with the median age of occurrence being between 60 and 70 years of age^[1].

1.1.1 Types of DLBCL

Being a widely-heterogeneous entity in several respects, the foremost being genetic, DLBCL has proven difficult to stratify into multiple distinct, well-defined subtypes, giving rise to drastically differing treatment outcomes in patients treated in the same manner^[2]. Owing to its heterogeneity, most cases of DLBCL belong to the group: DLBCL, not otherwise specified (DLBCL-NOS). The remaining minority of DLBCL cases are stratified into other groups established by WHO, such as primary DLBCL of the central nervous system, primary cutaneous DLBCL, leg type, DLBCL associated with chronic inflammation, or Epstein-Barr-virus-positive DLBCL-NOS, etc.^[3].

According to WHO, DLBCL-NOS (henceforth referred to as DLBCL) is further classified into two distinct types according to cell of origin (COO) and gene expression profiling (GEP): the germinal center B-cell-like (GCB) and the activated B-cell-like (ABC) type^[2-4]. Different types of DLBCL originate from B-lymphocytes at distinct stages of development (Fig. 1) that have undergone the process of malignant transformation. The GCB type of DLBCL originates from germinal center B-cells and is typically characterized by high expression levels of the transcription repressor BCL6, and hypermutated immunoglobulin genes. The ABC type of DLBCL stems from activated peripheral blood B-cells, more precisely from plasmablasts that haven't terminally differentiated into plasmacytes. Its major defining characteristics are constitutive B-cell receptor (BCR) activation, stimulating the NF- κ B pathway via the Bruton tyrosine kinase (BTK), and the overexpression of drivers of plasmacytic differentiation, such as IRF-4^[2,4,5].

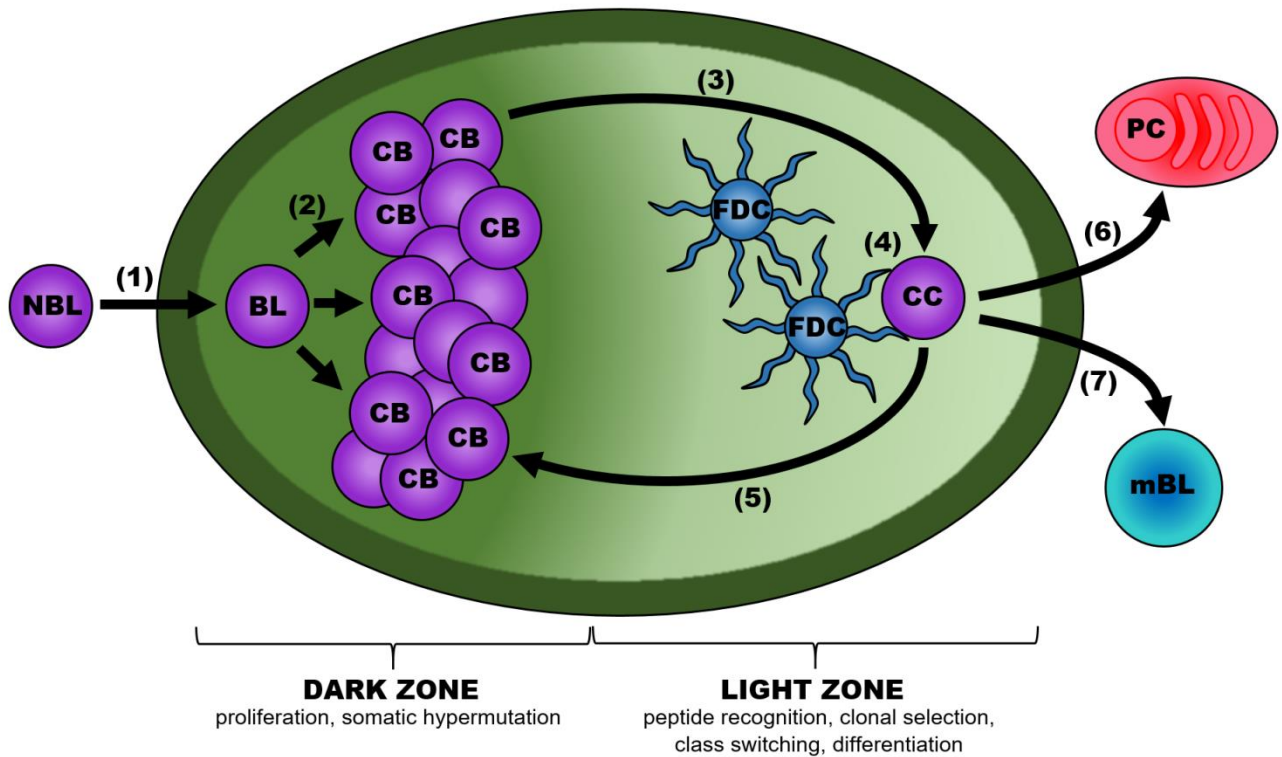


Figure 1. Differentiation of germinal center B-lymphocytes. NBL - naive B-lymphocyte; BL - B-lymphocyte; CB - centroblast; CC - centrocyte; FDC - follicular dendritic cell; PC - plasmacyte; mBL - memory B-lymphocyte. A naive B-lymphocyte enters the germinal center of a lymph node (1) and begins to proliferate in the dark zone, creating centroblasts (2). During proliferation, centroblasts undergo somatic hypermutation, generating clones of B-lymphocytes coding for antibodies with differing affinities for antigen. Centroblasts then move to the light zone, where they express the antibody on their surface, thus becoming centrocytes (3). Follicular dendritic cells present antigen and survival signals to centrocytes, which selects for centrocytes with the highest affinities for the presented antigen (4). Centrocytes with weak affinity to the antigen die by apoptosis (not shown). Further refinement of a centrocyte's antigen affinity is accomplished by returning to the dark zone and undergoing another cycle of somatic hypermutation (5). This can happen several times before a centrocyte is signaled to exit the germinal center and differentiate either into a plasmacyte (plasmablast stage not shown) (6) or a memory-B-lymphocyte (7). Taken and adapted from Allen et al. (2007)^[6].

Histologically, DLBCL manifests as large, diffusely-arranged B-cells of almost exclusively either centroblastic, immunoblastic, or anaplastic morphological variants (Fig. 2), with a nuclear size equal to or exceeding normal macrophage nuclei^[4].

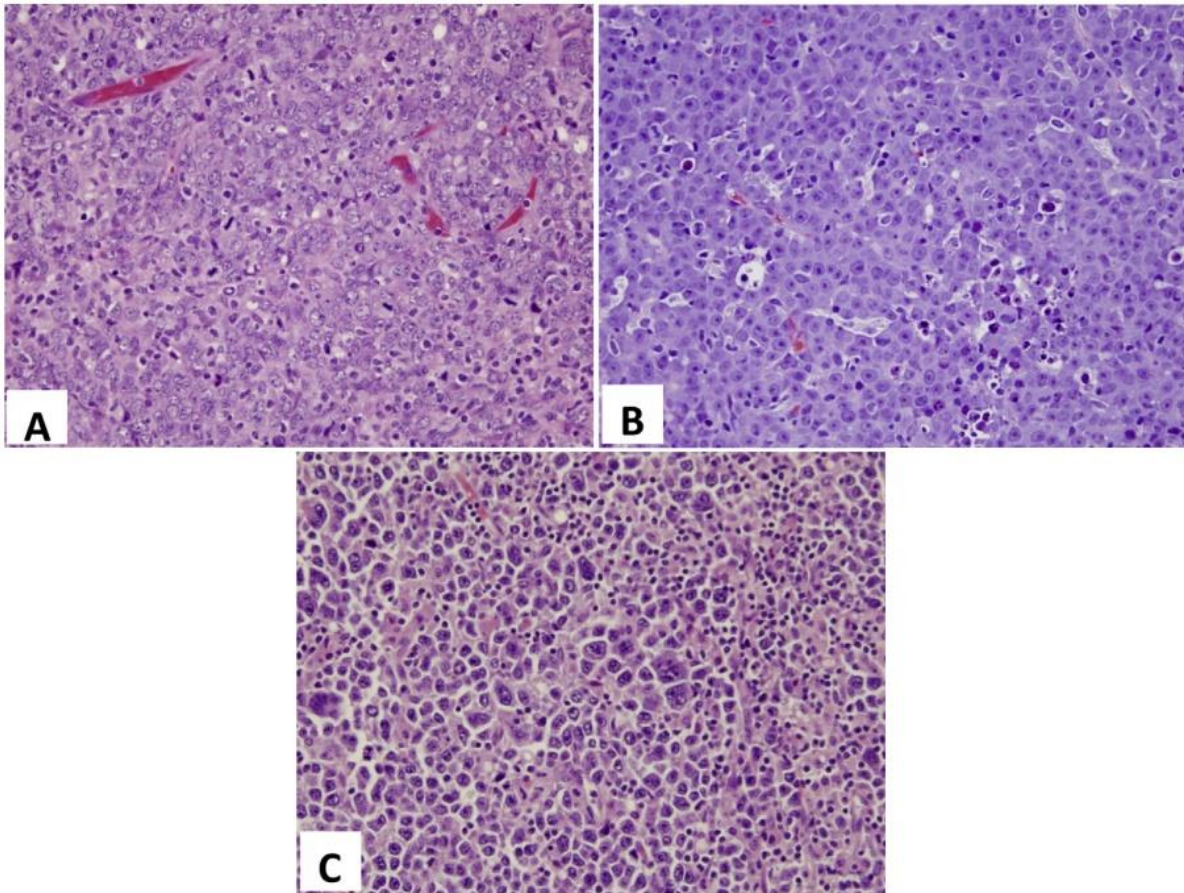


Figure 2. Morphologically distinct variants of DLBCL. (A) Centroblastic variant - large cells with vesicular nuclei and chromatin, and two to three membrane-bound nucleoli. (B) Immunoblastic variant - large cells with moderate-to-abundant basophilic cytoplasm. The nucleus contains a centralized nucleolus, often with thin protrusions of chromatin extending to the nuclear membrane. (C) Anaplastic variant - large or very large cells with pleomorphic nuclei, often in a sinusoidal pattern^[4]. Taken and adapted from Li S et al. (2018)^[7].

In clinical practice, the determination of DLBCL subtype is routinely performed on tumor tissue samples using standardized immunohistochemical diagnostic procedures such as the Hans algorithm (Fig. 3). The Hans algorithm was developed as a less-demanding, low-cost alternative to cDNA-microarray-based GEP for the classification of DLBCL into GCB and non-GCB types, where the non-GCB type encompasses ABC-DLBCL and entities similar to it. The classification method relies on a set of three tissue section immunostainings which take advantage of antibodies specific to CD10, BCL6 and MUM1^[8]. These proteins have been highly-associated with either type of DLBCL by cDNA microarray studies^[2,9]. CD10 is a membrane-associated neutral endopeptidase^[10] whose expression in reactive or hyperplastic lymphoid tissues is restricted to germinal center B-lymphocytes^[11], which has been associated with better overall survival (OS)^[8]. A DLBCL section is considered CD10-positive if 30 % or more of the cells in the sample show staining. The tumor is subsequently classified as GCB-DLBCL. If the threshold of CD-10 staining is not reached, the next step in the algorithm is the evaluation of the degree of BCL6 expression in the tumor. Within the B-lymphocyte lineage, BCL6 is detectable only in germinal center B-lymphocytes^[12], where it regulates the formation of the germinal center^[13] by acting as a transcription repressor^[14]. Overexpression of BCL6 in DLBCL predicts for better OS. If the proportion of BCL6-stained cells in the tumor section is less than 30 %, the DLBCL is classified as non-GCB. If, however, the immunoreactivity threshold is reached, a final assessment of DLBCL type is done by observing MUM1/IRF-4 staining, due to BCL6 expression itself not being specific to GCB-DLBCL^[8]. MUM1, or interferon regulatory factor 4, is a transcriptional activator^[15] specifically expressed in plasma cells, a small subset of germinal center B-lymphocytes and in activated T-lymphocytes^[16]. A DLBCL sample with over 30 % of cells stained for MUM1/IRF-4 is classified as non-GCB, which is associated with significantly worse OS^[8]. The Hans algorithm is concordant with GEP approximately 86 % of the time^[17].

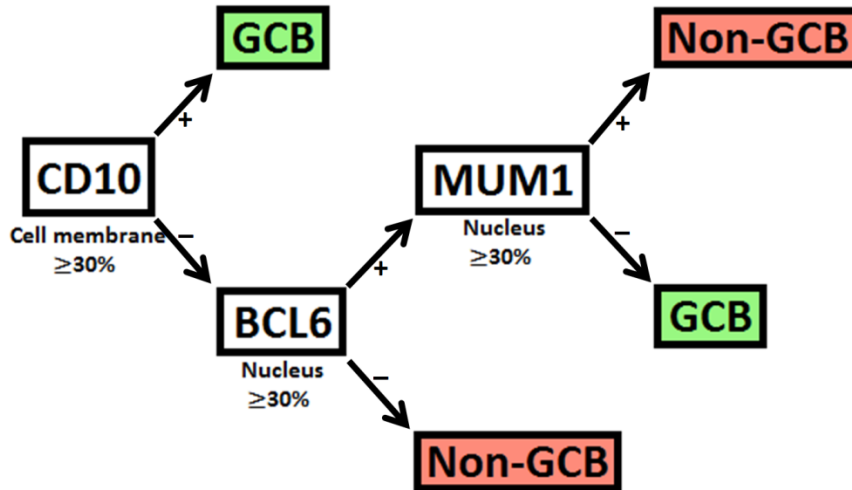


Figure 3. Schematic of the Hans IHC algorithm. Percentages below white boxes represent cut-offs for a positive signal. Taken and adapted from Hans et al. (2004)^[8].

Because the Hans algorithm left room for improvement of classification accuracy, several other immunohistochemical algorithms were subsequently developed^[17-19]. The Choi algorithm (Fig. 4), although not used in clinical practice, was developed due to the major improvements in the treatment of DLBCL and the emergence of improved antibodies specific for germinal center B-lymphocytes. The Choi algorithm, similarly to the Hans algorithm, uses antibodies against CD10, BCL6 and MUM1/IRF-4, but with the addition of antibodies against GCET1 and FOXP1 to classify cases of DLBCL according to COO with more specificity. Although Choi et al. (2009) report the GEP concordance rate of their algorithm to be significantly higher than that of the Hans algorithm (93 %)^[18], an independent study by Meyer et al. (2011) that characterized the same samples (among more others) showed the difference in GEP concordance to be less substantial (86 % vs. 87 %)^[17].

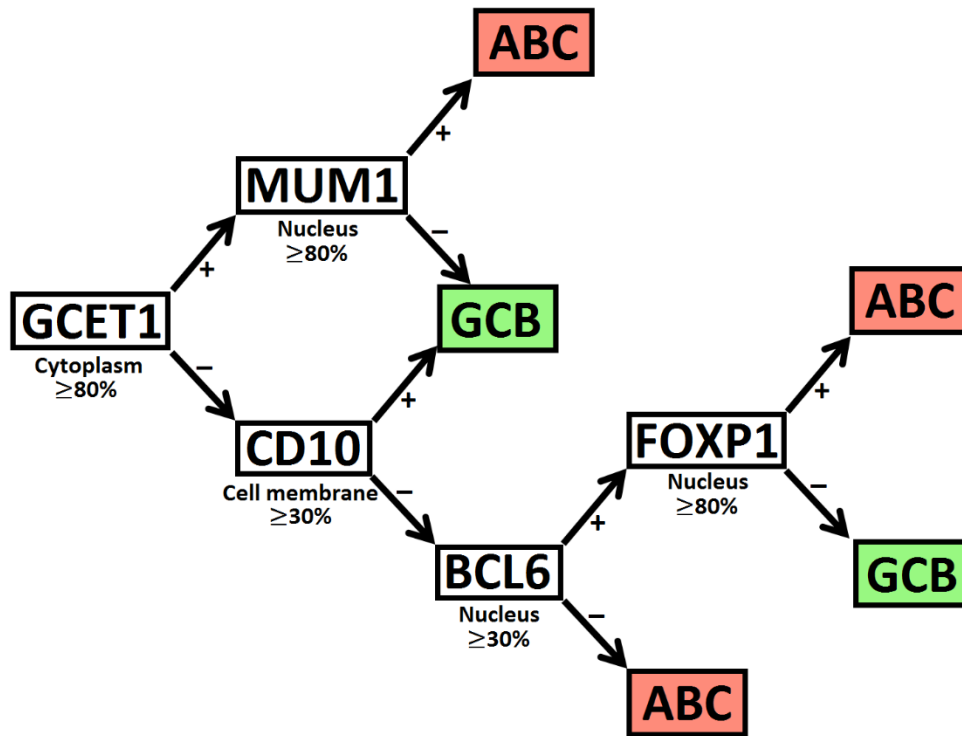


Figure 4. Schematic of the Choi immunohistochemical algorithm. Percentages below white boxes represent cut-offs for a positive signal. Taken and adapted from Choi et al. (2009)^[18].

Meyer et al. (2011) have also designed an immunohistochemical algorithm for DLBCL classification, called the Tally algorithm (Fig. 5). The algorithm disregards sequential estimation of gene expression and instead relies on a cumulative expression score of observed COO-specific markers. If more GCB-specific markers than ABC-specific markers show expression levels above the 30 % cell staining threshold, the tumor is classified as GCB-DLBCL and vice versa. If an equal number of expression markers are present, the expression of LMO2 is used as a tiebreaker. The predictive power of the Tally algorithm is estimated to be only slightly weaker than that of the Choi algorithm^[17] and is not used in routine clinical settings.

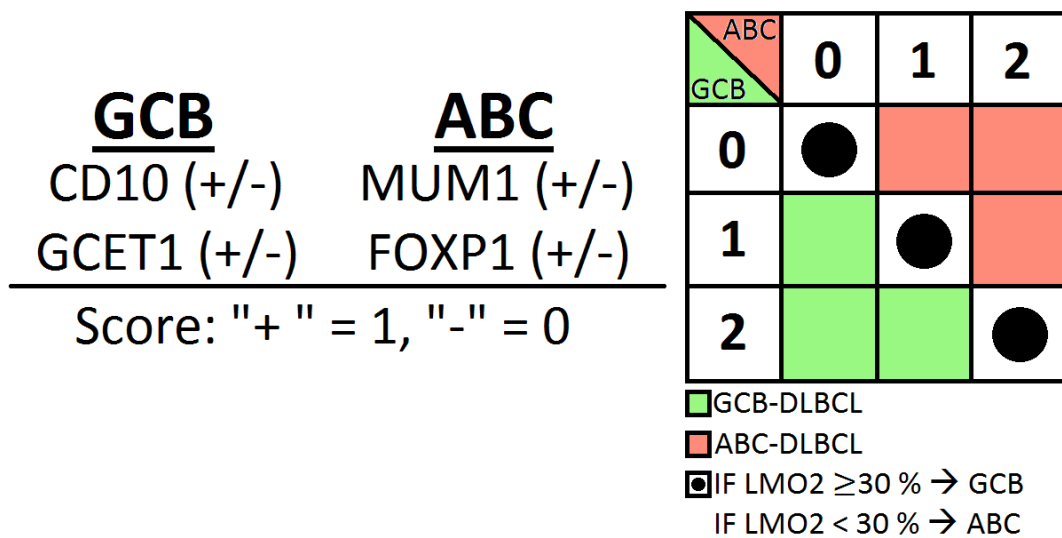


Figure 5. Schematic of the Tally immunohistochemical algorithm. The cut-off for a positive signal is 30 % of stained cells. Taken and adapted from Meyer et al. (2011)^[17].

Because COO assignment by immunohistochemical methods frequently shows poor reproducibility due to technical, procedural and interobserver variability^[20], further studies correlating expression of multiple genes to the COO have resulted in the development of more accurate DLBCL classification methods. The Lymph2Cx assay is a gene expression assay based on the NanoString Counter gene expression system^[20,21]. The assay assigns COO classification to DLBCL cases by analyzing the mRNA expression levels of 15 genes differentially expressed between ABC and GCB in samples of formalin-fixed paraffin-embedded tissue. A weighted average of the mRNA expression levels of the genes is used to generate a predictor score. An additional five housekeeping genes in the panel serve as a sample quality control. The Lymph2Cx assay was reported to show a >95% COO assignment concordance with cDNA microarrays^[20].

1.1.2 Staging and Prediction of Clinical Outcome

The Ann Arbor system used in modern-day lymphoma staging was created in 1971^[22] and further refined in 1989^[23] in order to stratify Hodgkin's lymphoma patients into prognostic subgroups. The classification of the disease into one of four stages is based upon the number and location of cancer tissue growths within the body, along with observed lymphoma-related symptoms^[23]. Due to the difference between the ways Hodgkin's lymphoma and NHL spread throughout the body, the Ann Arbor system was deemed insufficient by itself for prognostic stratification of NHL patients^[24], and a more accurate prognostic model for aggressive NHLs, called the international prognostic index (IPI), was developed in 1993^[25].

The IPI assigns patients to clinical risk groups based on a cumulative scoring approach which takes five universally-recognized clinical features into account and assigns one point for each present risk factor. Risk factors are: age greater than 60, tumor stage of III or higher, an elevated serum lactate dehydrogenase level, more than one extranodal site, and an Eastern Cooperative Oncology Group (ECOG) performance status between 2 and 4. Patients are stratified into four prognostic risk groups according to the number of points: low risk (0-1 points), low-intermediate risk (2 points), high-intermediate risk (3 points), and high risk (4-5 points). An age-adjusted IPI, which doesn't take age or the number of extranodal sites into account, was developed alongside IPI for use in prognostic classification of younger patients. Younger patients are stratified the same way as older patients, but with only one point of difference between risk groups (0, 1, 2 or 3)^[25].

In the time since the creation of the IPI, therapy for DLBCL has improved considerably. This had put the prognostic power of the IPI into question and prompted a revision of the risk classification system based on a redistribution of the IPI scoring system^[26]. However, some of the clinical prognostic factors that were previously important for patient risk assessment had become less relevant^[27]. This resulted in the creation of the National Comprehensive Cancer Network (NCCN) - IPI using statistical modeling. The NCCN-IPI is based on the same clinical features as IPI, but uses a refined categorization of age and normalized LDH, and only takes sites in the bone marrow, central nervous system, gastrointestinal tract/liver, and lungs into account when scoring extranodal tumor involvement. Although patients are stratified into the same four groups as in IPI, NCCN-IPI better discriminates between high and low risk, and high-intermediate and high risk prognostic groups^[28]. Although improvements of the prognostic stratification of NHL patients based on clinical features have been suggested, the IPI still remains in routine use^[29].

Even though the IPI is successfully used for risk assessment in routine clinical settings, it does not take the wide genetic heterogeneity of DLBCL into account, which leaves much room for improvement. In recent years, much effort has been devoted to the discovery of prognostic factors in DLBCL using gene expression profiling and has produced actionable results^[30]. So far, the only gene-expression-based predictor of therapeutic outcome in use is COO classification, where ABC-type DLBCL is generally associated with having a poorer outcome than GCB-type DLBCL^[9,31].

1.1.3 Signaling Pathways Commonly Altered in GCB-DLBCL

Germinal center B-cell-like DLBCL often harbors mutations resulting in dysregulated B-cell homing^[32], PI3K/Akt pathway dysfunction^[33,34], and aberrant epigenetic modification^[35-37].

Dysregulation of B-cell homing in GCB-DLBCL can be mediated by mutations in the *S1PR2*, *GNAI3* and *GNAI2* genes^[32]. The *S1PR2* gene encodes for the sphingosine-1-phosphate receptor protein 2 (S1PR2) - a high-affinity heterotrimeric G-protein-coupled receptor^[38]. Signaling through S1PR2 serves to restrict B-lymphocytes to lymph node germinal centers^[39] by means of a sphingosine-1-phosphate gradient^[40]. The $G_{\alpha 2}$ and $G_{\alpha 13}$ subunits of heterotrimeric G proteins, encoded by the *GNAI2* and *GNAI3* genes, respectively, are downstream mediators of S1PR2 signaling^[32,39]. Mutations in each of the three genes serve in the egress of neoplastic B-lymphocytes from germinal centers, and are enriched in GCB-DLBCL^[32,37].

The dysfunction of the PI3K/Akt pathway in GCB-DLBCL is predominantly caused by loss-of-function aberrations of PTEN by means of somatic mutations and heterozygous deletions^[34]. The primary consequence of PTEN loss is the constitutive activation of Akt, which results from the build-up of phosphatidylinositol-(3,4,5)-trisphosphate, bound by Akt's pleckstrin homology domain. This, in turn, promotes cellular metabolism and protein synthesis through the effects of mTOR, inhibits apoptosis, and activates the cell cycle by inhibiting key regulatory proteins^[41]. Another outcome of Akt activation is the upregulation of MYC, which results from suppression of the phosphatase activity of GSK3 β ^[34].

Aberrations in epigenetic modification are more commonplace in GCB-DLBCL than ABC-DLBCL^[35-37], where they contribute to the irregular activation or repression of genes. The *CREBBP*, *EP300*^[35], *EZH2*^[36], and *MEF2B*^[37] genes each play distinct, yet interconnected roles in the maintenance of the epigenome.

The proteins coded by the *CREBBP* and *EP300* genes (CPB and p300) share a large amount of both structural and functional similarity. Both belong to the KAT3 family of histone/protein lysine acetyltransferases and play a role in both epigenetically-driven^[42] and transcription-factor-driven control of protein expression^[35]. Most *CREBBP* and *EP300* mutations affect the acetyltransferase domain and are often heterozygous, suggesting, through haploinsufficiency, that the proteins serve as tumor suppressors. The mutated acetyltransferase domain has a reduced affinity for acetyl-CoA. Besides being unable to acetylate histone proteins, mutated CPB and p300 have lost the ability to acetylate p53 and BCL6^[35]. Because the acetylation of p53 by CPB/p300^[43] serves to disrupt the interaction of p53 and Mdm2^[44], *CREBBP* and *EP300* mutations lead to decreased tumor suppressor activity of p53^[35]. BCL6 is involved in the control of the cell cycle, differentiation and apoptosis in B-lymphocytes of the germinal center^[45]. Acetylation of BCL6 by CBP/p300 inhibits its function as a transcriptional repressor^[35,46], thus the loss of the acetyltransferase function of CBP/p300 promotes uncontrolled B-lymphocyte proliferation^[35].

MEF2B encodes for a transcription factor (MEF2B)^[47] which regulates transcription both by association with histone acetylases, such as p300^[48], and calcium-dependent association with histone deacetylases through Cabin1^[49,50]. MEF2B has been implicated in lymphomagenesis through its ability to promote transcription from the *BCL6* promoter in DLBCL. N-terminal mutations have been observed to abrogate the binding of Cabin1 to MEF2B, which eliminates both the suppression of p300 binding to MEF2B and indirect binding of transcription-repressing histone deacetylases through Cabin1^[51]. Somatic mutations in *MEF2B* were found to be more common in the GCB subtype of DLBCL^[37,51].

The *EZH2* gene encodes a histone N-methyltransferase (EZH2) which tri-methylates lysine 27 of histone 3 (H3K27) as the catalytic subunit of the polycomb repression complex 2^[52]. Heterozygous somatic missense mutations affecting Tyr641 in the active site of EZH2 have been observed to occur frequently in GCB-DLBCL, with 21.7 % of cases positive for the mutation, and do not occur in ABC-DLBCL^[36]. The mutations modify the substrate specificity of EZH2, decreasing its ability to methylate unmethylated and monomethylated histone proteins, and simultaneously increasing its affinity towards dimethylated H3K27, resulting in an increase of hypermethylation in mutant-bearing cells^[53]. These findings, along with the fact that EZH2 is involved in the silencing of antiproliferative genes in B-lymphocytes^[54] strongly implicate the hypermethylation-inducing EZH2 mutations in lymphomagenesis.

1.1.4 Signaling Pathways Commonly Altered in ABC-DLBCL

The survival of ABC-type DLBCL is dependent on the constitutive activity of the transcriptional activator NF- κ B^[55,56], which is accomplished via several different genetic aberrations^[57-60]. Common causes of constitutive NF- κ B activation in ABC-DLBCL are mutations affecting signal transduction proteins within and downstream of the B-cell receptor (BCR)^[57,58]. The B-cell receptor is a multimeric complex on the surface of B-lymphocytes. It consists of an antigen-binding immunoglobulin molecule non-covalently bound to a disulfide-linked CD79A/CD79B heterodimer which contains immunoreceptor tyrosine-based activation motifs (ITAMs)^[61]. Binding of antigen to multiple BCRs promotes clustering of the receptors and proximity-induced phosphorylation of ITAM domains on the CD79A/CD79B heterodimer by Src-family kinases^[62]. This, in turn, facilitates the binding of downstream effector kinases, such as SYK and BTK, which serves as a trigger for the activation of several cellular pathways^[63], which results in NF- κ B activation by means of CARD11-mediated activation of the I κ B kinase^[57].

CD79B mutations are found in about a fifth of ABC-DLBCL cases, but are known to also be found in GCB-DLBCL, albeit much more rarely. *CD79A* mutations are also more commonly found in ABC-DLBCL, but in a considerably lower number of cases^[57]. The Lyn tyrosine kinase associates with and phosphorylates tyrosine residues in the ITAM motifs of CD79B, which is required for the internalization of the BCR complex^[64,65]. Mutations in the *CD79A* and *CD79B* genes often affect the ITAM motif, either by replacing the tyrosine with another amino acid or by deleting the part of the motif that contains the phosphorylation site. As a consequence, these mutations disturb the interaction between Lyn and CD79B, thus promoting constitutive expression of the BCR on the cell surface^[57].

CARD11 is a cytoplasmic scaffold protein consisting of a CARD, coiled-coil, and MAGUK domain^[66]. It functions downstream of the BCR and lays in a dormant state due to the association of its CARD and coiled-coil domains with an inhibitory domain. When the linker region of CARD11, positioned between the coiled-coil and MAGUK domains, is phosphorylated, CARD11 forms the multi-protein CBM complex with BCL10 and MALT1 (among others) through coiled-coil domain interactions, which serves to activate the IKK complex, removing inhibition of NF- κ B^[67]. *CARD11* mutations predominantly affect the coiled-coil domain and are present in approximately 10 % of ABC-DLBCL and 4 % of GCB-DLBCL^[58]. Mutations in the coiled-coil domain of CARD11 disrupt the association between the inhibitory and coiled-coil domains, allowing association with MALT1 and BCL10 without the need for phosphorylation^[68].

Another process resulting in constitutive NF- κ B activation common in ABC-DLBCL is mediated by mutations in *MYD88*^[60]. MYD88 associates with toll-like receptors through its toll/interleukin-1 receptor (TIR) homology domain, acting as a signal transduction protein. It then recruits the IRAK4/1 complex via its death domain, which, through TRAF6-mediated polyubiquitylation, activates the IKK complex, leading to NF- κ B activation^[69]. Mutations in *MYD88* occur in about 40 % of ABC-DLBCL. The L265P variant constitutes approximately three quarters of *MYD88* mutations in ABC-DLBCL, and is rarely observed in GCB-DLBCL. Other *MYD88* mutations are, however, nearly equally distributed among DLBCL subtypes. The L265P amino acid substitution affects an evolutionarily-conserved residue within the TIR domain, facilitating the formation of the MYD88/IRAK4/1 complex by an, as of yet, unknown mechanism^[60].

TNFAIP3 is involved in NF- κ B regulation by means of its dual ubiquitylation and deubiquitylation functions. The N-terminal domain of the protein removes ubiquitin residues from lysine 63 of RIP1, a mediator of TNF α -induced NF- κ B signaling, thereby abolishing its interaction with NEMO, a subunit of the IKK complex. Additionally, the C-terminal domain of TNFAIP3 polyubiquitylates lysine 48 of RIP1, leading to its proteasomal degradation^[70]. TNFAIP3's deubiquitylation activity also targets NEMO itself^[71], which is polyubiquitylated by the CBM complex beforehand in order to activate NF- κ B^[72]. Alterations of the *TNFAIP3* gene are almost exclusive to the ABC subtype of DLBCL, with about 30 % of cases carrying a mutation. All of the mutations found in *TNFAIP3* are inactivating, making TNFAIP3 either highly-unstable or dysfunctional^[59].

Lastly, differentiation from germinal center B-lymphocytes into plasma cells is often halted in ABC-DLBCL^[73]. The *PRDM1/BLIMP1* gene codes for a transcriptional repressor required for the termination of BCR signaling and proliferation in germinal center B-lymphocytes, leading to their terminal differentiation into antibody-secreting plasma cells^[74]. Since GCB-DLBCLs originate from cells that normally don't express PRDM1/BLIMP1, abnormal inactivation of the protein's function is restricted to the ABC subtype. Biallelic inactivating mutations in *PRDM1/BLIMP1* are present in about a quarter of ABC-DLBCL, giving rise to the conclusion that the gene is a tumor suppressor. However, up to about 80 % of cases demonstrate a lack of PRDM1/BLIMP1 protein expression, with most ABC-DLBCL still expressing the appropriate mRNA. This suggests that the protein's inactivation in most cases of ABC-DLBCL is a consequence of impaired translation and/or protein stability caused by external mechanisms^[73].

1.1.5 Courses of Treatment

In the late 20th century, DLBCL, or as it was known back then: diffuse histiocytic non-Hodgkin's lymphoma, was routinely treated with either radiotherapy^[75], or single-agent chemotherapy^[76]. In the following years, a combination-chemotherapy regimen consisting of cyclophosphamide, doxorubicin, vincristine, and prednisone (CHOP) was deemed the best option for treatment of DLBCL patients, as it managed to achieve complete remission in 45-55 % of patients^[77].

The current standard treatment for DLBCL patients is a combination of rituximab and CHOP (R-CHOP). Rituximab is a murine/human chimeric monoclonal antibody specific for the CD20 antigen bound to the outer surface of B-lymphocytes with therapeutic activity in B-lymphocytic malignancies^[78]. It was approved for the treatment of relapsed, low-grade, or follicular NHLs in 1997 by the United States Food and Drug Administration and by the European Medicines Agency less than a year later. In 2006, it was greenlit for aggressive NHL therapy in combination with CHOP^[79]. Sixty to seventy percent of patients who undergo R-CHOP treatment have a 5-year progression-free survival, though 30-40 % of them ultimately relapse with refractory disease^[80].







1.2 The BTB-kelch Protein Family and Kelch-Repeat Superfamily

The first member of the BTB (broad-complex, tramtrack and bric-a-brac) -kelch protein family: "kelch", was discovered in ring canals of *Drosophila melanogaster* egg chambers^[81], where it mediates the organization of F-actin filaments^[82]. The name stems from the German word for goblet, given to the gene as a result of egg shells of homozygous mutant females often having an anterior opening, thus resembling a cup^[83]. Since then, many structurally and functionally diverse proteins possessing kelch repeats have been discovered, prompting their categorization under the name: kelch-repeat superfamily^[84].

1.2.1 The Structure of Kelch-Repeat Proteins

Five distinct protein families characterized by specific arrangements of structural domains constitute the kelch-repeat superfamily (Table 1). These protein families are: the N-dimer, C-propeller, or BTB/Kelch family; the C-propeller family; the N-propeller, C-coiled coil family; the N-propeller family; and the propeller protein family^[84]. Most metazoan and, more specifically, human kelch-repeat proteins belong to the BTB-kelch protein family^[85].

Table 1. Common arrangements of domains in kelch-repeat proteins, with examples listed. The first group of kelch-repeat proteins (N-dimer, C-propeller proteins) have a C-terminal BTB/POZ (Poxvirus and Zinc-finger) domain and an N-terminal kelch domain comprised of four to six kelch motifs, and is otherwise known as the BTB-kelch protein family. The second group (C-propeller proteins) is composed of proteins with a C-terminal kelch domain containing between five and seven kelch motifs. The proteins of the third group (N-propeller, C-dimer proteins), structured from an N-terminal kelch domain containing six kelch repeats and an extended C-terminal coiled-coil domain, have so far been identified exclusively in yeasts. Group four proteins (N-propeller proteins) share only the N-terminal kelch domain. Proteins consisting almost exclusively of kelch repeats arranged in one or two kelch domains (propeller proteins) are the sole constituents of the fifth group. Taken and adapted from Adams et al. (2000)^[84].

Subgroup	Protein (# of kelch motifs)	Length (aa)	Species
N-BTB, C-Kelch 	Calicin (6) ENC-1 (6) IPP (6) Keap1/KIAA0132 (6) Kelch (6) Kel-1 (6) Mayven (6) NRP/B (6) NS1-BP (5) Poxvirus ORFS (4-6) Sarcosin (5)	588 589 584 624 688 618 593 589 589 ~600 596	Human, bovine Human, mouse Human, mouse Human, mouse <i>D. melanogaster</i> <i>C. elegans</i> Human Human Human Vaccinia, Shope, etc. Human
C-Kelch 	Actin-fragmin kinase (6) Galactose oxidase (7) Muskelin (6) SPE-26 (5)	737 639 735 570	<i>P. polycephalum</i> <i>D. dendroides</i> Mouse <i>C. elegans</i>
N-Kelch, C-coiled coil 	Kel1p (6) Kel2p (6) Teal (6)	1164 882 1147	<i>S. cerevisiae</i> <i>S. cerevisiae</i> <i>S. pombe</i>
N-Kelch 	Attractin (7) HCF-1 (6) HCF-2 (6) LZTR-1 (2) Mahogany (7) RAG-2 (6) Ral2p (3)	1198 2035 792 552 1336 527 611	Human, mouse, <i>C. elegans</i> Human Human, <i>C. elegans</i> Human Mouse Human, mouse <i>S. pombe</i>
Single-Kelch only 	P40 (6)	372	Human
Dual-Kelch only 	α -Scruin (12) β -Scruin (12)	918 916	<i>L. polyphemus</i> <i>L. polyphemus</i>

The kelch motif, a 44-56 amino-acid-long four-stranded β -sheet, is present in all proteins of this superfamily. Multiple consecutively-chained instances of this motif are found at either the amino or carboxy terminal of the protein, forming a three-dimensional structure within the kelch domain called the “ β -propeller” (Fig. 6A). Within the β -propeller, the kelch motifs assume a radial distribution, laying tilted to a central axis, with each kelch motif forming one “blade” of the propeller^[84,86]. There is modest-to-low sequence similarity between kelch motifs of the same protein, and even lower sequence similarity between kelch motifs of different proteins. However, eight conserved residues can be found within most kelch motifs: four hydrophobic residues preceding a double-glycine residue, and two distant aromatic residues spaced apart by different, though often recurring, lengths of amino acid sequence^[84,85,87]. The BTB/POZ domain (henceforth referred to as the BTB domain) is the characteristic structural element of the BTB-kelch family of kelch-repeat proteins, consisting of 120 amino acids^[84,88]. Most of the BTB domain is taken up by its core made of multiple α -helices, on either side of which is a small β -sheet. The arrangement of the BTB domain’s secondary structure elements allow it to form homodimers with biaxial symmetry (Fig. 6B)^[89]. Depending on residues within the interaction surface of the domain, different BTB domains can interact, allowing the formation of protein heterodimers^[88]. Similarly to the kelch domain, several conserved residues are found within BTB domains of different proteins, most of which are buried within the domain’s core^[89].

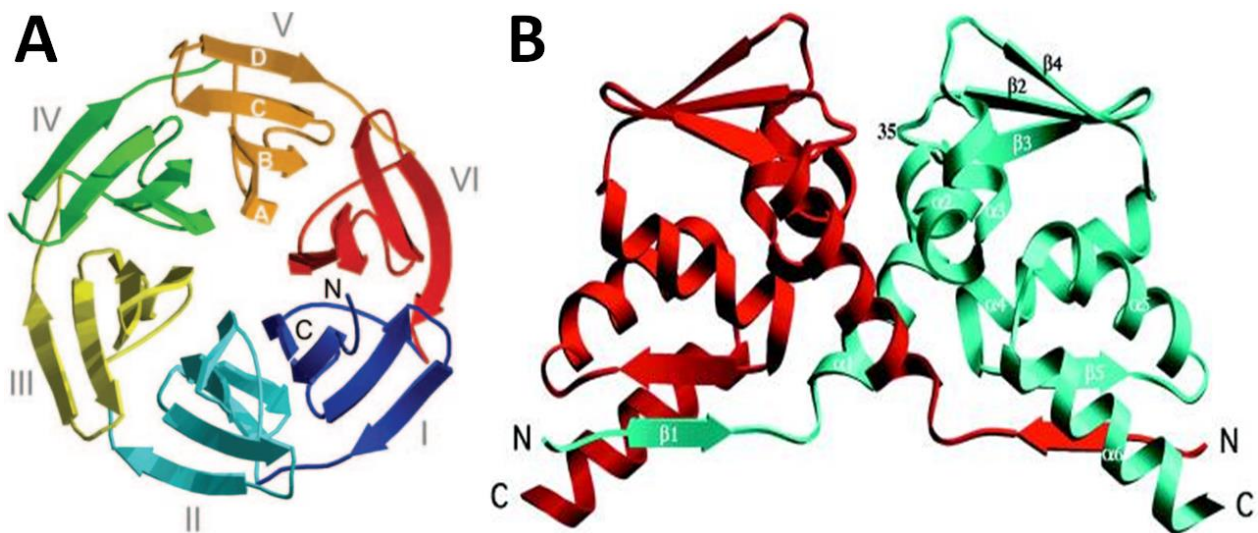


Figure 6. Ribbon diagrams of (A) the kelch domain of human kelch-like ECH-associated protein 1 (KEAP1), taken from Li et al.(2004)^[90], and (B) the BTB domain of the human promyelocytic leukemia zinc finger (PLZF) protein, taken from Ahmad et al. (1998)^[89].

1.2.2 The Functions of Kelch-Repeat Proteins

As compiled by Adams, Kelso, and Cooley (2000), kelch-repeat proteins mediate a diverse set of cellular and extracellular processes, such as the formation and organization of cytoskeletal elements (IPP/KLHL27, ENC1/KLHL37, etc.), modification of cellular morphology (β -Scrutin, calicin, etc.), regulation of gene expression (KEAP1/KLHL19, RAG-2, etc.), primary alcohol oxidation (e.g. galactose oxidase), and so forth^[84].

Several members of the kelch-like protein (KLHL) subfamily of BTB-kelch proteins have been observed to associate with the cullin-3 (Cul3) based E3 ubiquitin ligase, such as KLHL2^[91], KLHL11^[92], KLHL19 (better known as KEAP1)^[93], and KLHL20^[94]. Cullin-RING ubiquitin ligases are comprised of a catalytic RING-finger protein, a substrate adaptor protein, and a Cullin protein, which acts as a scaffold, connecting the catalytic and substrate-specifying parts of the complex^[95]. The association between KLHL family proteins and Cul3 is mediated by their BTB domains. A number of KLHL family proteins act as substrate-specific adaptors in the Cul3-based ubiquitin ligase proteolysis pathway^[96,97].

1.3 Kelch-Like Protein 6

Kelch-like protein 6 (KLHL6) was originally discovered in ovine ileal Peyer's patches using cDNA subtraction, and its expression in humans was subsequently localized to germinal center B-cells^[98]. Expression of the protein is persistent throughout the entirety of B-cell development, with increased expression during antigenic stimulation of B-cells within the germinal center^[98]. Inside the cell, KLHL6 localizes mostly to perinuclear areas^[99].

1.3.1 Structure of KLHL6

Although the exact tertiary structure of the protein is still unknown, KLHL6 was shown to contain an N-terminal BTB domain, along with a C-terminal kelch domain consisting of six kelch repeats^[98], categorizing it as a member of the BTB-kelch family of kelch-repeat proteins^[84]. Besides the BTB and kelch domains, KLHL6 contains an intervening BTB and C-terminal kelch (BACK) domain, as do all other kelch-like proteins^[96,99,100]. The BACK domain is 130 amino acids long, fully α -helical in structure, and has multiple highly-conserved residues^[92,100]. The most notable role of the BACK domain is the formation of a Cul3-binding cleft together with the BTB domain, reinforcing the interaction with the E3 ubiquitin ligase^[92].

1.3.2 Proposed Roles of KLHL6 in the Cell

It was demonstrated that, in KLHL6^{-/-} mice, the absence of KLHL6 impairs the maturation of B-lymphocytes in the bone marrow past the pre-B-cell stage, resulting in shrinkage of the spleen. B-cell receptor signaling and the germinal center formation in peripheral lymph nodes are negatively-affected as well^[99,101]. Although it has been shown that KLHL6 isn't indispensable for germinal center formation^[99,101], but is necessary for the survival and development of T1 B-lymphocytes^[101], the exact function of the protein is yet to be determined^[99,101]. Speculation has yielded opinions that KLHL6 may be an adaptor for the Cul3 ubiquitin ligase, with substrate specificity for a protein involved in BCR signaling^[99] or B-cell-activating-factor-mediated B-cell maturation^[101].

1.3.3 KLHL6 in Malignancies

The observed involvement of KLHL6 in the B-cell maturation process^[99,101] is supported by the fact that it is frequently found mutated in several types of neoplasms stemming from mature B-lymphocytes, such as chronic lymphocytic leukemia^[102,103], marginal zone lymphoma^[104], follicular lymphoma^[105], and even in acute myeloid leukemia, though at much lower frequencies^[106]. The highest frequency of KLHL6 mutations, however, is observed in DLBCL, with about 10 % of patients carrying a mutation^[30,107-110]. The most common KLHL6 mutant variants in DLBCL are Leu65Pro, Leu90Phe, Glu547Lys, and Glu568Lys^[30,107,109].

1.4 Drug Sensitivity Score

The complexity of sample-dose-response matrices resulting from high-throughput drug screening of cells often calls for the reduction of the dose dimension into a single parameter, such as the IC₅₀. This often offers limited insight into differences between drug responses of cancer and normal cells^[111]. The drug sensitivity score (DSS) condenses the characteristics of a drug response curve into a single value which can be used to easily identify druggable vulnerabilities in cancer samples, or observe changes in drug sensitivity between test and control samples^[112].

1.4.1 The Mathematics Behind the Drug Sensitivity Score

The DSS is a quantitative drug response metric based on closed-form integration of the area under an interpolated dose-response curve. Multiple parameters of a dose-response curve (IC₅₀ (inflection point), slope, maximum and minimum asymptote) are estimated through a logistic function model and integrated into a single variable. A non-linear dose-response function is first used on the observed drug response data to model the response function as a continuous function of the dose, producing a dose-response curve (a - maximal response/top asymptote of the drug response curve; b - slope of the drug response curve; c - half-maximal inhibitory concentration (IC₅₀); d - minimum response/bottom asymptote of drug response curve; x - drug concentration (x₁ to x₂ - active concentration range); y - response function)^[112]:

$$y = d + \frac{a - d}{1 + 10^{b(c-x)}}$$

The area under the curve, which is the area between the x-axis and the dose-response curve, is then calculated as a closed-form exact solution of a definite integral with a set minimum drug activity level defining the starting and ending concentrations (t - minimum activity level of drug; AUC - area under the curve)^[112]:

$$AUC = \int_{x_1}^{x_2} y(x) dx = Y(x_2) - Y(x_1)$$

$$Y(x) = \frac{(a - d) \log_{10}(1 + 10^{b(c-x)})}{b} + ax$$

$$x_1 = c - \frac{\log_{10}(a - t) - \log_{10}(t - d)}{b}$$

$$AUC = a \left[x_2 - c + \frac{\log_{10}(1 + 10^{b(c-x_2)}) + \log_{10}(1 - \frac{t}{a})}{b} \right]$$

Finally, the DSS is calculated by subtracting the integrated area below the minimum drug activity level from the area under the curve, and dividing the resulting value by the maximum possible response area^[112]:

$$DSS_1 = \frac{AUC - t(x_2 - x_1)}{(100 - t)(C_{max} - C_{min})}$$

A normalization of the DSS calculation by the logarithm of the top asymptote (DSS_2) serves to select against drugs which show only off-target effects^[112]:

$$DSS_2 = \frac{DSS_1}{\log_{10} a}$$

A further normalization of DSS_2 by the dose range over which the response exceeds the activity threshold (DSS_3), is used to emphasize drugs with a wide therapeutic window^[112]:

$$DSS_3 = DSS_2 \frac{x_2 - x_1}{C_{max} - C_{min}}$$

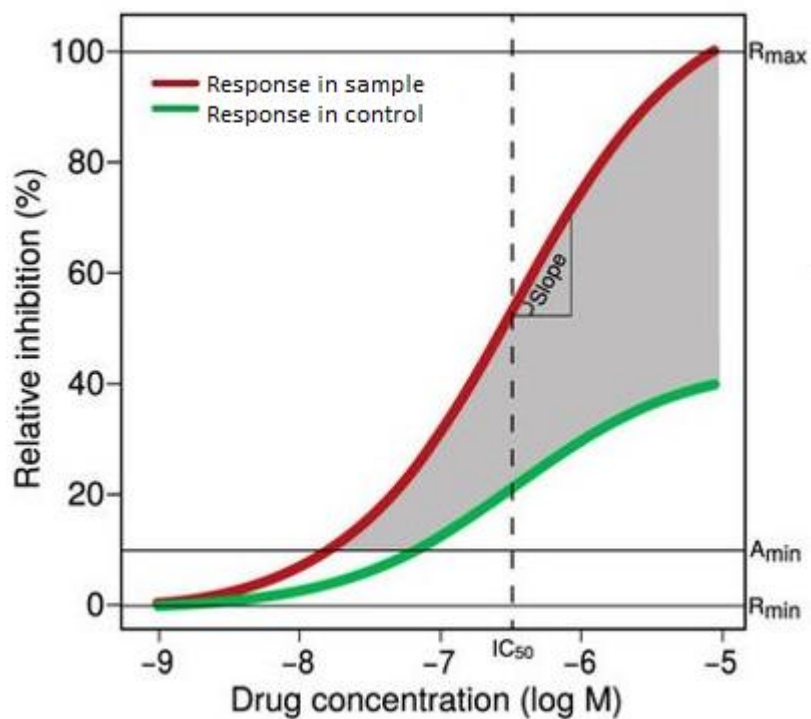


Figure 7. Graphical representation of the differential drug sensitivity score calculation. R_{\min} - minimal observed response; R_{\max} - maximal observed response; A_{\min} - designated minimal drug activity level. The gray area represents the AUC used for dDSS calculation. Taken and adapted from Yadav et al. (2014)^[112].

2. AIM OF THE STUDY

The aim of this study was to detect the cellular pathways the KLHL6 protein is involved in, and potentially define its exact cellular function, based on the results of drug sensitivity and resistance testing.

3. MATERIALS AND METHODS

3.1 Materials

3.1.1 The SU-DHL-4 Cell Line

In 1976, “diffuse histiocytic lymphoma” cells from a peritoneal effusion of a male 38-year-old were used for the establishment of the Stanford University-diffuse histiocytic lymphoma-4 (SU-DHL-4) human cell line^[113]. The cell line is classified as a DLBCL of the GCB subtype and carries an EZH2 Y641S mutation^[114]. The cell line displays immunoglobulin G molecules with kappa light chains on its surface. It has a translocation affecting the BCL2 gene, placing it under the control of the immunoglobulin heavy chain promoter (t(14;18)(q32;q21))^[113]. The SU-DHL-4 cell line is negative for the Epstein-Barr virus, hepatitis B and C viruses, human immunodeficiency viruses 1 and 2, and the human T-lymphotropic virus^[114].

3.1.2 The SU-DHL-5 Cell Lines

The Stanford University-diffuse histiocytic lymphoma-5 (SU-DHL-5) human cell line was established in 1978 from a lymph node biopsy sample of a female 17-year-old “malignant diffuse histiocytic lymphoma” patient^[113], which was later reclassified as GCB-type DLBCL^[115]. The cell line has no *Bcl-2*, *c-Myc*, or *Bcl-6* translocations, and displays immunoglobulin M molecules with lambda light chains on its surface^[113]. It is negative for the Epstein-Barr virus, hepatitis B and C viruses, human immunodeficiency viruses 1 and 2, and the human T-lymphotropic virus^[115].

SU-DHL-5 cells were transduced with lentiviral constructs prior to this study. The cells were transduced with either of the following expression constructs: a *KLHL6* gene mutated by site-directed mutagenesis (see below) of *KLHL6* cDNA extracted from SU-DHL-4 cells, cDNA of a wild-type *KLHL6* gene extracted from SU-DHL-4 cells, or a construct expressing only emerald green fluorescent protein (EmGFP). All transduced genes were placed under the control of a constitutively active EF-1 α promoter of the pLEX_307^[116] lentiviral expression vector. The constructs carrying *KLHL6* genes had a streptavidin-hemagglutinin (str/HA) dual-tag at the 3' end of the gene. Four most common *KLHL6* missense mutations in DLBCL were chosen for transduction into SU-DHL-5 cells: Leu65Pro (L65P), Leu90Phe (L90F), both found in the BTB domain of the protein, and Glu547Lys (E547K) and Glu568Lys (E568K), which both affect the kelch domain, giving a total of six derivative SU-DHL-5 cell lines established by transduction. The SU-DHL-5 cell lines expressing these six proteins will henceforth be referred to as: S5-EmGFP, S5-KLHL6-wt, S5-KLHL6-L65P, S5-KLHL6-L90F, S5-KLHL6-E547K, and S5-KLHL6-E568K.

3.2 Methods

3.2.1 Maintenance of SU-DHL-5 Cell Cultures

Prior to their use in this study, all aforementioned SU-DHL-5 cells were kept frozen in fetal bovine serum (FBS) (Thermo Fisher Scientific, United States) with 10 % V/V dimethyl sulfoxide (DMSO) (MP Biomedicals, United States) at -150°C. An untransduced SU-DHL-5 cell line was maintained along with transduced ones. Thawing was performed according to the following protocol: a cryogenic vial (True North™, Heathrow Scientific, United States) containing a 1 mL aliquot of frozen cells was thawed in a heated water bath. The aliquot was transferred to a polypropylene tube. Five milliliters of Roswell Park Memorial Institute (RPMI) 1640 medium (Corning, United States), supplemented with 20 % V/V FBS (Thermo Fisher Scientific, United States), 1 % V/V penicillin/streptomycin (10,000 units/mL penicillin, 10,000 µg/mL streptomycin) (Thermo Fisher Scientific, United States) and 1% V/V L-alanyl-L-glutamine dipeptide (200 mM in 0.85% NaCl) (GlutaMAX™-I 100X, Thermo Fisher Scientific, United States) (henceforth referred to as RPMI-20-FBS) were added onto the aliquot and mixed by slowly inverting the tube a number of times. The aliquot was centrifuged at 126 G for 3 minutes at RT. After removing supernatant, the cell pellet was resuspended in 6 mL of fresh RPMI-20-FBS (supplemented with 0.5 µg/mL of puromycin (Merck, United States) if the cells carried a lentivirally-transduced construct). The suspension was transferred to a 25 cm² cell culture flask (Nunc™ EasYFlask™ Nunclon™ Delta Surface, Thermo Fisher Scientific, United States) and placed into a cell culture incubator at 37°C and 5 % V/V CO₂. The next day, 4 mL of RPMI-20-FBS medium (supplemented with 0.5 µg/mL of puromycin (Merck), where appropriate) were added to the cell culture. Cells were passaged at least twice after thawing before being used in any experiments.

Cell cultures were split into halves or thirds every two or three days, respectively. This was done according to the following procedure: cells were thoroughly resuspended, transferred to plastic tubes, and centrifuged at 300 G for 5 minutes at room temperature (RT). Supernatant was removed by vacuum. Depending on the splitting ratio, two or three milliliters of fresh RPMI-20-FBS (with or without puromycin, depending on transduction status) were used to resuspend the cell pellet. One milliliter of cell suspension was placed into a cell culture flask (Nunc™ EasYFlask™ Nunclon™ Delta Surface, Thermo Fisher Scientific, United States) filled with either 9 or 14 milliliters of the same medium used for resuspension, and placed into a cell culture incubator at 37°C and 5 % V/V CO₂. Cells to be used in DSRT or proliferation testing were cultured in puromycin-free medium for at least two passages prior to the procedure.

Aliquots of maintained cell lines were frozen in FBS with 10 % V/V DMSO throughout the study, using the following protocol: cell lines to be aliquoted and frozen had been passaged the day before. After resuspension, 5 mL of a cell culture were transferred to a polypropylene tube and centrifuged at 126 G for 3 minutes at RT. Supernatant was removed by vacuum. Cell pellets were resuspended using 1 mL of FBS with 10 % V/V DMSO. The cell suspension was transferred to a small cryogenic vial (True North™, Heathrow Scientific, United States), placed into a freezing container, and placed into a freezer set to -70°C. The next day, the container was transferred to a second freezer set to -150°C.

3.2.2 Extraction of DNA from Cells for Cell Line Authentication

Cultures of untransduced SU-DHL-4 and SU-DHL-5 cell lines were resuspended thoroughly. A 15 µL aliquot of each cell suspension was placed into a small polypropylene tube. The same volume of Trypan Blue stain (0,4%, Thermo Fisher Scientific, United States) was added to the cell aliquots. Two 10 µL aliquots of each mixture were placed into dual-chambered cell counting slides (Countess™, Thermo Fisher Scientific, United States). The density and viability of cells were determined using an automated cell counter (Countess™, Thermo Fisher Scientific, United States) and averaged over the duplicates.

Aliquots of SU-DHL-4 and SU-DHL-5 cultures containing $1.0 \cdot 10^7$ live cells were placed into polypropylene tubes and centrifuged at 300 G for 5 minutes. Supernatant was removed using vacuum. Cell pellets were resuspended in 1 mL of ice-cold 1x phosphate-buffered saline, transferred to 1.5 mL polypropylene tubes and centrifuged at 300 G for 5 minutes. Supernatant was vacuumed away. DNA was extracted from the cell pellets using the NucleoSpin® Tissue kit (Macherey-Nagel, Germany) according to the following protocol: each cell pellet was resuspended in 200 µL of “T1” lysis buffer. Twenty-five microliters of “Proteinase K” and 200 µL of “B3” lysis buffer were added to each cell suspension. The suspensions were briefly vortexed and then incubated at 70°C for 12 minutes in a heating block. Two hundred and ten microliters of 100 % ethanol were added to each sample. The samples were vortexed vigorously, then applied to NucleoSpin® Tissue Columns placed into NucleoSpin® Tissue Collection Tubes and centrifuged for one minute at 11,000 G. The columns were placed into new collection tubes and 500 µL of “BW” wash buffer were added to each column. The columns were then centrifuged for one minute at 11,000 G. Six hundred microliters of “B5” wash buffer were added to each column. The columns were centrifuged for one minute at 11,000 G twice, with flowthrough being removed between centrifugations. The columns were transferred to 1.5 mL polypropylene tubes and 100 µL of “BE” elution buffer were added to each column. The columns were incubated at RT for one minute, then

centrifuged for one minute at 11,000 G. The concentration and purity of each DNA sample were determined using a spectrophotometer (NanoDrop 8000, Thermo Fisher Scientific, United States). The samples were sent to the Genomics Unit of the Technology Centre at the Institute for Molecular Medicine Finland (FIMM), where DNA-based authentication of the cell lines was performed using the GenePrint24 system (Promega, United States), which is based on the measurement of the lengths/numbers of repeats of 24 short tandem repeat sequences using capillary electrophoresis.

3.2.3 Extraction of Total Cytosolic Protein from Cells

The following procedure was performed twice, both during and after cessation of puromycin treatment of transduced SU-DHL-5 cells. Cell density and viability of SU-DHL-5 cell line cultures were determined using an automated cell counter (Countess™, Thermo Fisher Scientific, United States) as previously described. Pellets were made from aliquots of 5.0×10^6 live cells by the same method used in DNA extraction. Total cytoplasmic protein was extracted from the cell pellets using the NE-PER® Nuclear and Cytoplasmic Extraction Reagents kit (Thermo Fisher Scientific, United States) according to the manufacturer's instructions. Protein isolates made from SU-DHL-5 cell cultures undergoing puromycin treatment were stored at -70°C , while isolates from SU-DHL-5 cells grown in puromycin-free medium for three passages were made ten days later and used for protein quantification on the same day, along with the protein isolates from puromycin-treated SU-DHL-5 cells.

3.2.4 Protein Quantification

A protein concentration standard ranging from 0.2 mg/mL to 2.0 mg/mL was made using bovine serum albumin (Biowest, France) dissolved in "CERII" extraction buffer from the NE-PER® Nuclear and Cytoplasmic Extraction Reagents kit (Thermo Fisher Scientific, United States). Five microliters of protein standard and SU-DHL-5 cytoplasmic protein isolate were pipetted in triplicate into a clear 96-well microplate (SpectrPlate™, 96 MB, PerkinElmer, United States) and treated with reagents from the DC Protein Assay Kit (BioRad, United States) according to the manufacturer's instructions. Absorbances were measured at a wavelength of 750 nm using a microplate reader (FLUOstar Omega, BMG Labtech, Germany). The averaged absorbances of the standards were used to construct a curve from which protein concentrations of the cytoplasmic protein samples were extrapolated.

3.2.5 Western Blotting

A volume containing approximately 14.3 μg of protein was transferred from each SU-DHL-5 cytoplasmic protein isolate to a small polypropylene tube. Extraction buffer (CERII) from the NE-PER[®] Nuclear and Cytoplasmic Extraction Reagents kit (Thermo Fisher Scientific, United States) was added to protein aliquots up to a total sample volume of 12 μL . Samples were mixed with 4x Laemmli buffer (BioRad, United States) (277.8 mM Tris-HCl (pH 6.8), 44.4 % V/V glycerol, 4.4 % V/V lithium dodecyl-sulfate, 0.02% V/V bromphenol blue, in H₂O) with 10 % V/V 2-mercaptoethanol (14.2 M, BioRad, United States) in a 3:1 sample to buffer volume ratio and placed in a heating block set to 95°C for 5 minutes.

A pre-cast 4-15 % polyacrylamide gradient gel with 15 μL wells (Mini-Protean[®] TGX[™], BioRad, United States) was placed into the scaffold of an electrophoresis cell (Mini PROTEAN[®] 3, BioRad, United States). The inner compartment of the scaffold was then filled with 1x tris/glycine/sodium dodecyl sulphate buffer (25 mM Tris, 192 mM glycine, 0.1 % SDS, pH 8.3). The buffer was used to clear the wells of any residual matter from the gel's packaging. Twelve microliters of protein samples were pipetted into the wells of the gel, and 2.5 μL of a protein molecular mass marker (Precision Plus Protein[™] Dual Color Standard, BioRad, United States) were pipetted into the leftmost empty well. The samples were electrophoresed for 75 minutes using a voltage of 100 V. The gel was removed from its plastic casing, the wells were cut off, and the gel was placed onto the nitrocellulose membrane of a Trans-Blot[®] Turbo[™] Mini Nitrocellulose Transfer Pack (BioRad, United States). The transfer pack containing the gel was placed into a Trans-Blot[®] Turbo[™] electrophoretic transfer system (BioRad, United States) and the "1 MINI TGX (2.5 A, 25 V, 3 min)" setting was chosen.

After the transfer procedure, the membrane was trimmed, then washed twice for 5 minutes on a platform rocker using small amounts of tris-buffered saline (0.15 M NaCl, 50 mM Tris, pH 7.6) with 0.1 % V/V polysorbate 20 (Tween[®]20) (MP Biomedicals, United States) (henceforth referred to as 0.1 % TBST). Most of the liquid was then drained, and 5 mL of 5 % w/V skimmed milk powder (Valio Ltd., Finland) dissolved in 0.1 % TBST were used for blocking. After one hour of blocking on a platform rocker at RT, the blocking solution was removed, and the membrane was subjected to three washing steps on a platform rocker using small volumes of 0.1 % TBST, each lasting 10 minutes at RT. A mix of two primary antibodies dissolved in blocking solution was added onto the membrane: a monoclonal rabbit anti-HA-tag antibody (C29F4, Cell Signaling Technology, United States) diluted in a 1:2000 ratio, and a monoclonal mouse anti- β -actin antibody (AM4302, Thermo Fisher Scientific, United States) diluted in a 1:5000 ratio. The membrane was

incubated in the antibody solution on a platform rocker overnight in the dark at 4°C. The primary antibody mix was removed from the membrane and three 10-minute washing steps were performed on a platform rocker at RT with small amounts of 0.1 % TBST. The membrane was then incubated in the dark for one hour at RT on a platform rocker with a solution of two secondary antibodies dissolved in blocking buffer. The secondary antibodies were: a polyclonal goat anti-rabbit-immunoglobulin-G (heavy and light chain) antibody with an attached Alexa Fluor[®] 700 fluorophore (A-21038, Thermo Fisher Scientific, United States), and a polyclonal donkey anti-mouse-immunoglobulin-G (heavy and light chain) antibody with an attached IRDye 800CW fluorophore (926-32212, LI-COR Biosciences, United States), both diluted in a 1:10.000 ratio. The membrane was imaged using 10-minute exposures to 685 and 785 nm wavelength light, using the Odyssey FC imaging system (LI-COR biosciences, United States).

Signal intensities were quantified using Image Studio Lite 5.2.5 (LI-COR biosciences, United States). Relative expression levels of HA-tagged KLHL6 proteins were calculated by normalization of KLHL6 protein bands to corresponding beta-actin bands.

3.2.6 Mycoplasma Infection Assay

Aliquots of cleared medium taken from cultures of SU-DHL-5 cell lines carrying transduced constructs were tested for *Mycoplasma* infection using the MycoAlert[™] Mycoplasma Detection kit (Lonza, Switzerland), according to the following protocol: two milliliters of cell culture samples were centrifuged for five minutes at 200 G. One hundred microliters of the supernatants were transferred to the wells of a 96-well plate. MycoAlert[™] reagent, substrate and MycoAlert[™] Assay Control were reconstituted by the addition of MycoAlert[™] buffer and left to equilibrate at RT for 15 minutes. One hundred microliter aliquots of MycoAlert[™] buffer and Assay Control were placed into the 96-well plate as a negative and positive control, respectively. One hundred microliters of MycoAlert[™] reagent were added to each sample and incubated at RT for five minutes. The luminescence of the samples was measured. One hundred microliters of MycoAlert[™] substrate were added to each sample and incubated at RT for 10 minutes. The luminescence of the samples was measured. The protocol was performed using a white 96-well polypropylene microplate (Assay Plate, Corning, United States) and a microplate reader capable of luminescence quantification (FLUOstar Omega, BMG Labtech, Germany).

3.2.7 Cell Proliferation Assay

The cell density and viability of all transduced SU-DHL-5 cell lines were assessed using an automated cell counter as previously described (Countess™, Thermo Fisher Scientific, United States). Aliquots of the cell cultures containing 4.5×10^5 live cells were centrifuged at 300 G for 5 minutes. Supernatant was removed and pellets were resuspended using 4.5 mL of RPMI-20-FBS, creating cell suspensions containing 1.0×10^4 cells per 100 μ L. Cell suspensions containing 5.0×10^3 cells per 100 μ L were then made by mixing an aliquot of a suspension containing 1.0×10^4 cells per 100 μ L with an equal volume of RPMI-20-FBS. One hundred microliters of each cell line suspension were pipetted into the wells of a 96-well polypropylene microplate in triplicate (μ CLEAR®, model Cellstar® (655098), Greiner Bio-One, Austria). The microplate was placed into a cell culture incubator at 37°C and 5 % V/V CO₂ for 72 hours. Cells in the microplate were checked for abnormalities daily using a microscope (CKX41, Olympus, Japan).

After incubation, the microplate was taken to a darkened room and the CellTiter-Glo® 2.0 (CTG 2.0, Promega, United States) luminescence assay reagent was used to assay cell viability according to the following protocol: the plate containing the cells was equilibrated to RT for 30 minutes. Fifty microliters of CTG 2.0 were added to each well. The plate was wrapped in aluminium foil and placed on an orbital shaker set to 50 rpm for two minutes at RT. The foil-wrapped plate was taken off of the shaker and incubated at RT for 10 minutes. Luminescence was recorded using a microplate reader (FLUOstar Omega, BMG Labtech, Germany), with gain adjusted using the entire sample-bearing part of the microplate. Luminescence levels were averaged and used to determine cell proliferation rates.

3.2.8 Drug Sensitivity and Resistance Testing

The density and viability of cultured S5-EmGFP cells were determined using an automated cell counter (Countess™, Thermo Fisher Scientific, United States) as previously described. For the purpose of determining optimal cell plating density of transduced SU-DHL-5 cells in a 384-well microplate, an aliquot containing 1.25×10^6 live cells was pelleted, resuspended in 10 mL of fresh RPMI-20-FBS, and sent to the DSRT team of the High Throughput Biomedicine Unit of FIMM (henceforth referred to simply as the DSRT team), along with an aliquot of the same medium used to resuspend the cells. The cells were plated into a 384-well plate at densities of 1,250, 1,875, 2,500, and 3,125 cells per well and placed in a cell culture incubator at 37°C and 5 % V/V CO₂ for 72 hours.

Since the optimal plating density was determined to be 2,500 cells per well, an aliquot of 1.25×10^7 live cells was necessary for DSRT of each transduced cell line. All cell cultures had been kept in puromycin-free medium for four passages by this point. Cell density and viability were determined for all cultures of transduced SU-DHL-5 cells, except for the S5-KLHL6-E568K cell line. An aliquot of each cell line containing 1.25×10^7 live cells was pelleted, resuspended using 5 mL of RPMI-20-FBS, and transferred to a 175 cm² cell culture flask (Nunc™ EasYFlask™ Nunclon™ Delta Surface, Thermo Fisher Scientific, United States) containing 95 mL of RPMI-20-FBS, making a cell suspension containing 1.25×10^5 live cells per 1 mL. Culture flasks (five in total) were sent to the DSRT team.

Eight days prior to submitting the cells for DSRT, 528 different drugs dissolved in either DMSO or water were pre-printed into 384-well microplates using the Echo 550 and Echo 525 acoustic liquid handling devices (Labcyte, United States), respectively (list of drugs available online^[117]). Either 2.5 or 25 nL of a drug solution were dispensed into each well, with the volume dispensed depending on the drug itself. The drugs were printed in five concentrations spanning a ten-thousand-fold concentration range. The microplates containing the drugs were kept in pressurized StoragePods® (Roylean Developments, United Kingdom) in an atmosphere of inert nitrogen gas with less than 1 % oxygen and a relative humidity of 2 % or lower. During storage, the solvents had evaporated, leaving the drugs as dry powder at the bottom of the wells. Prior to the addition of cells, 5 µL of RPMI-20-FBS were added to each well in order to prime the microplates. After 20 minutes had passed, 20 µL of a single-cell culture containing 2,500 cells were added to each well using a MultiFlo FX microplate dispenser equipped with a RAD™ (random access dispense) module for mapped dispensing (BioTek, United States) using a 1-channel cassette. There were no replicates. The microplates were placed in a cell culture incubator at 37°C and 5 % V/V CO₂ and cultured for 72 hours.

After incubation, cell viability was assessed using the CTG 2.0 luciferase-based luminescence assay reagent (Promega) and a microplate reader. The assay results were used to construct drug response curves and consequently determine DSS values.

Differential drug sensitivity scores (dDSS) for cell lines expressing mutant KLHL6 proteins were calculated by subtracting the DSS of the mutant control sample (S5-KLHL6-wt) from that of a mutant test sample (SU-DHL-5 cells expressing mutant KLHL6). This can easily be interpreted as the difference in sensitivity to the applied compound between the test sample and control caused by each KLHL6 mutation. As a measurement of the influence of KLHL6 overexpression on drug sensitivity, additional dDSS calculations were made for the S5-KLHL6-wt cell line using the DSS values of the S5-EmGFP cell line as the overexpression control.

3.2.9 Verification of DSRT Results

Cell lines chosen for verification of DSRT results were the S5-EmGFP, S5-KLHL6-wt, S5-KLHL6-L65P, and S5-KLHL6-L90F cell lines. The cell cultures had been kept in puromycin-free medium for several passages by this point. Four drugs were chosen for result verification: GDC-0084 (Medchem Express, United States), Idelalisib (ChemieTek, United States), Ixabepilone (Medchem Express, United States) and Onalespib (Medchem Express, United States).

Viability and density of cell lines chosen for result verification were determined using an automated cell counter (Countess™, Thermo Fisher Scientific, United States) as described previously. An aliquot of 1.5×10^6 live cells was taken from each cell culture, pelleted and resuspended using 7.5 mL of RPMI-20-FBS, producing suspensions containing 2.0×10^5 cells per 1 mL.

Fifty microliters of the cell suspensions, containing 1.0×10^4 live cells, were pipetted into the wells of eight black 96-well polypropylene microplates (μ CLEAR®, model Cellstar® (655090), Greiner Bio-One, Austria) in triplicate. Four microplates contained S5-EmGFP and S5-KLHL6-wt cells, while the other four contained S5-KLHL6-L65P and S5-KLHL6-L90F cells. Each microplate was placed into a cell culture incubator at 37°C and 5 % V/V CO₂ immediately after filling all appropriate wells with cell suspension. The plating times were noted.

Aliquots of 10 mM GDC-0084, Idelalisib, Ixabepilone and Onalespib dissolved in DMSO were diluted in DMSO, then RPMI-20-FBS in such a way that the dilutions contained double the final amount of drug and 0.2 % V/V of DMSO. Solutions of 0.2 % V/V DMSO in RPMI-20-FBS and 20 μ M etoposide (Medchem Express, United States) dissolved in RPMI-20-FBS with 0.2 % V/V DMSO were used as the negative and positive controls, respectively. Each microplate was then taken out of the incubator separately for the administration of drug treatment. The time difference between cell plating and drug administration was kept as similar as possible for all microplates. By administering 50 μ L of a drug dilution to cells in the microplates, the drugs were diluted to their final concentrations (Table 2) and each well contained 0.1% V/V of DMSO. Each drug dilution was pipetted across a whole cell-bearing part of a microplate column, so that all drug treatments were done in triplicate. Each microplate was placed into a cell culture incubator at 37°C and 5 % V/V CO₂ immediately after all compounds were administered to it, and the starting time of incubation was noted. The plated cells were incubated at 37°C and 5 % V/V CO₂ for approximately 72 hours, with daily inspections performed in order to spot any contaminations or abnormalities.

The CTG 2.0 cell viability assay was performed on each microplate separately in a darkened room, in the same order as the plating/drug treatment done three days prior. Besides only 50 μ L of CTG 2.0 (Promega) reagent being added to each well instead of 100 μ L, the cell viability assay was done according to the manufacturer’s instructions as previously described. Only a single light gain adjustment was made for each pair of microplates containing cells treated with the same drug. Luminescence levels were then recorded using a microplate reader, averaged (FLUOstar Omega, BMG Labtech, Germany), adjusted to the negative control, and interpreted as percentages of cell viability. The resulting viability values were then sent to the DSRT team and used to make drug response curves and calculate DSS values. The verification of DSRT results of Ixabepilone treatment was done once more using the same protocol to ensure the validity of the results of the first verification experiment.

Table 2. Final concentrations of the drugs used in both DRST and result verification in nanomoles per liter [nM].

Drug	Concentrations used in DSRT [nM]	Concentrations used in DSRT result verification [nM]
GDC-0084	1, 10, 100, 1,000, 10,000	3, 10, 30, 100, 300, 1,000, 3,000, 10,000
Idelalisib	1, 10, 100, 1,000, 10,000	3, 10, 30, 100, 300, 1,000, 3,000
Ixabepilone	0.1, 1, 10, 100, 1,000	1, 3, 10, 30, 100, 300, 1,000

4. RESULTS

4.1 Preparation of Cells for Drug Screening

4.1.1 Cell Line Authentication

In order to check if any cross-contamination or other technical problems had occurred since their acquisition, such as the mislabeling of cell lines, a DNA-based cell authentication service was employed to confirm the identities of the SU-DHL-4 and SU-DHL5 cell lines.

Spectrophotometric analysis of DNA isolated from aliquots of SU-DHL-4 and SU-DHL-5 cell cultures showed good concentration and purity (Table 3).

Table 3. Absorbances, absorbance ratios and mass concentrations of DNA samples extracted from SU-DHL-4 and SU-DHL-5 cells.

Sample	A260	A280	A260/A280	A260/A230	Concentration [ng/ μ L]
SU-DHL-4	4.150	2.097	1.98	2.14	207.5
SU-DHL-5	2.576	1.292	1.99	2.29	128.8

The samples were then sent to a cell authentication service provided by the Genomics Unit of the Technology Centre at FIMM. The service cross-referenced the authentication results with several cell line databases (ATCC, JCRB, ICLC and DSMZ), as well as the Cellosaurus resource, giving an identity estimate of 100.0 % for the SU-DHL-4 cell line and 98.6 % for the SU-DHL-5 cell line (Table 4). Since the minimum of 80 % of matching alleles needed for confirmation according to the International Cell Line Authentication Committee (ICLAC) guidelines^[118] was surmounted in both cases, the cell lines were confirmed to be authentic.

Table 4. Expected and observed genetic profiles of SU-DHL-4 and SU-DHL-5 cell lines. Expected genotypes and identity estimates were inferred from information found in multiple cell line databases (ATCC, JCRB, ICLC, DSMZ, and Cellosaurus). Genotypes are presented as the number of short tandem repeat sequence repeats at the each screened locus. N/A - not applicable.

Locus	SU-DHL-4		SU-DHL-5	
	Expected Genotype	Observed Genotype	Expected Genotype	Observed Genotype
AMEL	X/Y	X/Y	X/X	X/X
CSF1PO	12/12	12/12	11/13	11/13
D10S1248	N/A	15/16	N/A	14/14
D12S391	N/A	18/20	N/A	20/24
D13S317	11/12	11/12	12/12	12/12
D16S539	11/13	11/13	11/13	11/13
D18S51	14/16	14/16	13/15	13/15
D19S433	N/A	14/15,2	N/A	13/14
D1S1656	N/A	15/18,3	N/A	12/12
D21S11	29/30	29/30	28/30	28/30
D22S1045	N/A	15/16	N/A	11/16
D2S1338	N/A	17/19	N/A	17/18
D2S441	N/A	11/14	N/A	11/13
D3S1358	15/16	15/16	15/16	15/16
D5S818	11/12	11/12	12/15	12/15
D7S820	8/11	8/11	10/10	10/10
D8S1179	13/13	13/13	13/15	13/14/15
DYS391	N/A	N/A	-/-	-/-
FGA	19/21	19/21	22/23	22/23
Penta D	9/14	9/14	11/12	11/12
Penta E	7/11	7/11	5/19	5/19
TH01	6/9,3	6/9,3	6/9	6/9
TPOX	9/11	9/11	8/8	8/8
VWA	18/19	18/19	17/17	17/17
Identity Estimate	100.0 %		98.6 %	

4.1.2 Cytoplasmic Protein Concentrations of Cell Lines

A standard curve representing absorbance as a function of protein concentration was constructed using bovine serum albumin solutions spanning a range of concentrations. The curve had an R-squared value of 0.9304 and intersected the ordinate at an absorbance value 0.1056. The concentration of each protein sample was inferred from measured absorbance values by using the function derived from the standard curve. The median of the protein concentrations was 1.69 mg/mL and the average was 1.79 mg/mL, with the lowest and highest concentrations being 1.19 mg/mL and 3.33 mg/mL, respectively (Table 5).

Table 5. Concentrations of cytoplasmic protein isolates made from cells of all SU-DHL-5 cell lines used in the study. Total cytoplasmic protein was isolated from the transduced cell lines both during and after puromycin treatment.

Puromycin Treatment	Cell Line	Protein Concentration [mg/mL]
No	SU-DHL5	3.33
	S5-EmGFP	1.72
	S5-KLHL6-wt	1.63
	S5-KLHL6-L65P	1.43
	S5-KLHL6-L90F	1.69
	S5-KLHL6-E547K	1.29
	S5-KLHL6-E568K	1.55
Yes	S5-EmGFP	1.73
	S5-KLHL6-wt	2.48
	S5-KLHL6-L65P	1.88
	S5-KLHL6-L90F	1.94
	S5-KLHL6-E547K	1.37
	S5-KLHL6-E568K	1.19

4.1.3 Confirmation of Expression Levels of KLHL6 Variants in SU-DHL-5 Cells

To ascertain if the transduction of SU-DHL-5 cells was successful, and whether expression levels of transduced str/HA-tagged KLHL6 proteins were stable and mutually similar after cessation of puromycin selection, western blotting was performed on samples of cytoplasmic protein extracted from each experimental SU-DHL-5 cell line, taken both during and after puromycin treatment of the transduced cells. Beta-actin was used as the loading control, and the protein samples from the untransduced SU-DHL-5 cell line and the S5-EmGFP cell lines were used as negative controls.

For the protein sample of the untransduced SU-DHL-5 cell line, as well as for both S5-EmGFP samples, neither of which had an HA-tag, the emission levels of the fluorescent anti-HA antibody located at the molecular mass of a band of HA-tagged KLHL6 protein were close to background. Comparatively, for SU-DHL-5 cell lines transduced with constructs carrying genes for HA-tagged KLHL6 proteins, bands containing the HA-tagged KLHL6 proteins were considerably more prominent (Fig. 8). Normalization of the fluorescence values was carried out as follows: all actin fluorescence levels were divided by the highest actin fluorescence level. Each resulting actin value was then multiplied by its corresponding fluorescence level of the HA-signal. The normalized HA-tag signals of cell lines expressing HA-tagged proteins were between 800 and 1,700 times stronger than the signal of the untransduced SU-DHL-5 cell line measured at the approximate same molecular mass (Table 6). This ratio, along with the low fluorescence levels of the negative controls, indicate high specificity of the anti-HA antibody and an absence of cross-contamination of cell lines and protein samples.

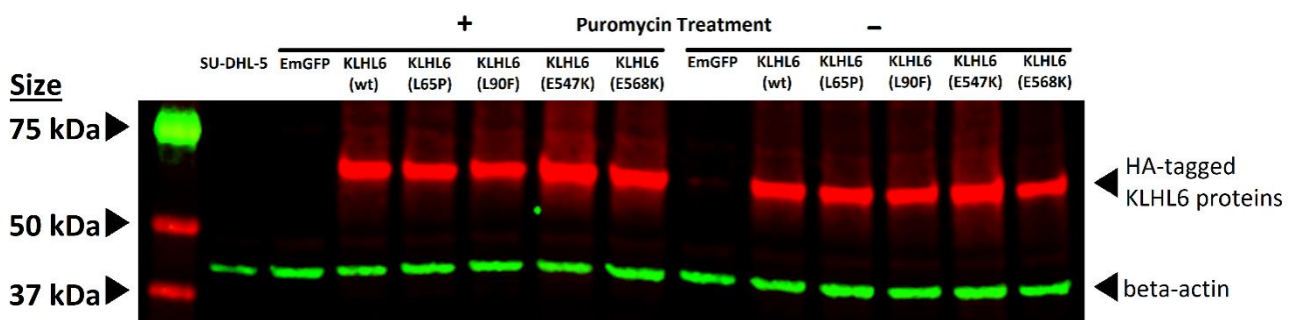


Figure 8. Expression of HA-tagged KLHL6 proteins and beta actin in cytoplasmic protein isolates extracted from cells of SU-DHL-5 cell lines. The lane marked “SU-DHL-5” contains protein isolate from cells of an untransduced SU-DHL-5 cell line. All other lanes contain protein isolates from SU-DHL-5 cells transduced with lentiviral constructs.

Table 6. Amount of fluorescence signal at each visible protein band of a western blot of cytoplasmic protein extracts made from transduced and untransduced SU-DHL-5 cell lines either during or after cessation of puromycin treatment. Quantified using Image Studio Lite 5.2.5 image processing software (LI-COR Biosciences, United States).

Puromycin Treatment	Cell Line	Fluorescence (HA-Tagged KLHL6 Proteins)	Fluorescence (Beta-Actin)	Fluorescence (HA-Tagged KLHL6 Proteins) (Normalized to Actin)
No	SU-DHL-5	0.02	0.00635	<0.01
Yes	S5-EmGFP	0.05	0.01	0.04
	S5-KLHL6-wt	14.3	0.00888	9.62
	S5-KLHL6-L65P	13.4	0.0101	10.25
	S5-KLHL6-L90F	10.7	0.0102	8.27
	S5-KLHL6-E547K	15.7	0.00919	10.93
	S5-KLHL6-E568K	13.3	0.0108	10.88
No	S5-EmGFP	0.65	0.0102	0.50
	S5-KLHL6-wt	14.2	0.0105	11.30
	S5-KLHL6-L65P	13.2	0.0128	12.80
	S5-KLHL6-L90F	12.2	0.0116	10.72
	S5-KLHL6-E547K	16.6	0.0132	16.60
	S5-KLHL6-E568K	11.6	0.011	9.67

The normalized signal strength of HA-tagged KLHL6 protein bands from cell samples of SU-DHL-5 cells kept in puromycin-free medium was on average 16 % stronger than that of their puromycin-treated counterparts (Fig. 9).

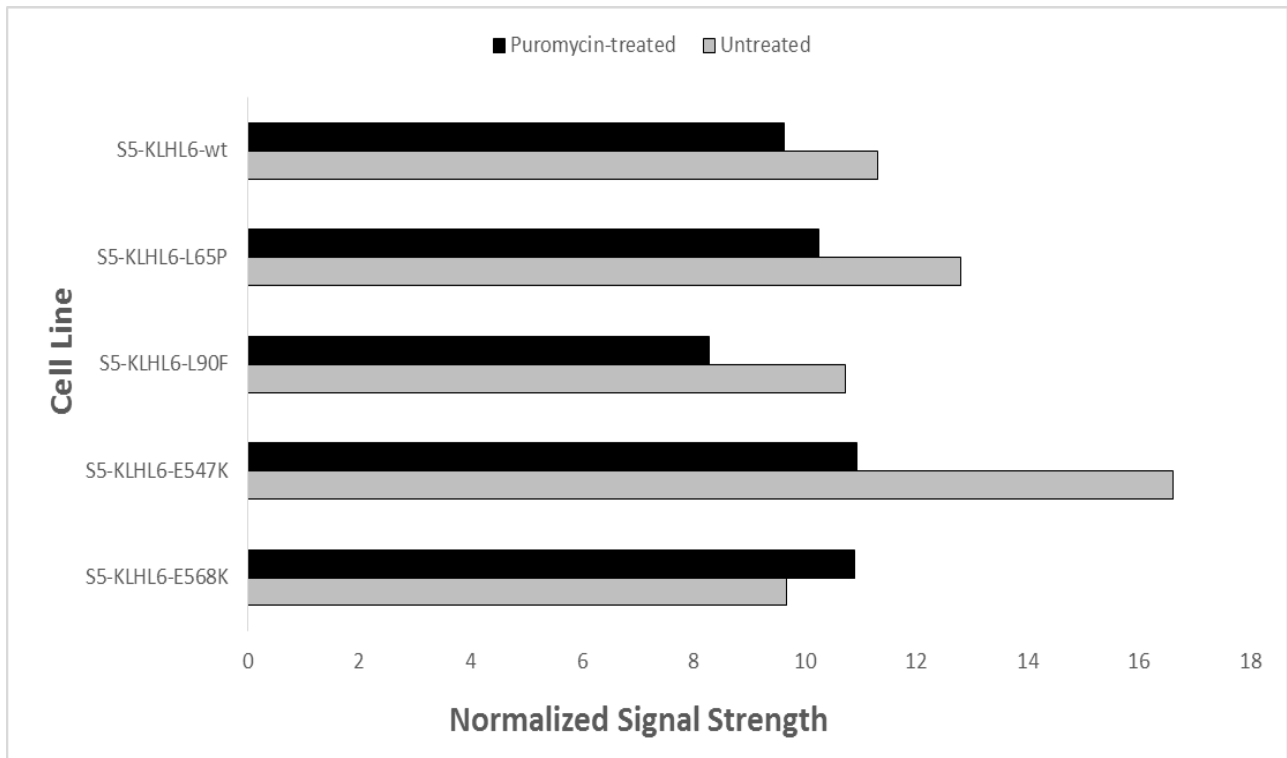


Figure 9. Relative expression levels of HA-tagged KLHL6 proteins in transduced SU-DHL-5 cell lines both during and after puromycin treatment. The values were calculated by normalizing signal strength of HA-tagged KLHL6 protein bands to those of corresponding beta-actin bands in a western blot.

The normalized signal strength values indicate high and mutually similar expression levels of recombinant KLHL6 variants in all transduced cell lines, confirming both successful transduction and stable expression after cessation of puromycin treatment.

4.1.4 Detection of Mycoplasma Infection of Cell Cultures

To ensure the cells were feasible for future drug screen experiments, cultures of transduced SU-DHL-5 cells were screened for the presence of an infection by species of *Mycoplasma* using a standardized luminescence-based reagent kit.

The levels of luminescence produced by the negative and positive controls corresponded with a negative and positive result, respectively, and luminescence levels of all samples of cell medium were well below the threshold of a positive result, confirming the absence of *Mycoplasma* infection (Table 7).

Table 7. Luminescence levels of cleared cell culture medium samples tested for presence of *Mycoplasma* using the MycoAlert™ mycoplasma detection kit (Lonza, Switzerland). Sample names correspond to the transduced SU-DHL-5 cell line culture the medium sample was taken from. A luminescence ratio of less than 0.9 is considered a negative result.

Sample	First Measurement of Luminescence Levels (MycoAlert™ Reagent Added)	Second Measurement of Luminescence Levels (MycoAlert™ Substrate Added)	Luminescence Level Ratio (2/1)
MycoAlert™ buffer (negative control)	977	338	0.345957
S5-EmGFP	14349	4682	0.326295
S5-KLHL6-wt	9242	4202	0.454663
S5-KLHL6-L65P	12886	4507	0.349759
S5-KLHL6-L90F	12381	4143	0.334626
S5-KLHL6-E547K	14904	6885	0.461957
S5-KLHL6-E568K	20629	9473	0.459208
MycoAlert™ positive control	181	2257	12.46961

4.1.5 Relative Proliferation Rates of Transduced Cells

Variability in proliferation rates between experimental cell lines would affect the interpretation of drug screening results, due to possible effects of lentiviral transduction or overexpression of KLHL6 and its mutant variants. I therefore assessed the proliferation rates of cells. I plated all transduced SU-DHL-5 cell lines and compared their proliferation rates before subjecting them to high-throughput drug screening.

The results of the luminescence assay implied similar proliferation rates between all transduced SU-DHL-5 cell lines for both cell densities used, except for the S5-KLHL6-E568K cell line, whose proliferation rate was on average 23.0 % slower than those of all the other cell lines plated at the higher density, and on average 29.2 % slower than those of all the other cell lines plated at the lower density (Fig. 10). This was later found to most likely be a result of erroneous cell counting prior to cell seeding for the experiment, and not a consequence of lentiviral transduction or KLHL6 overexpression.

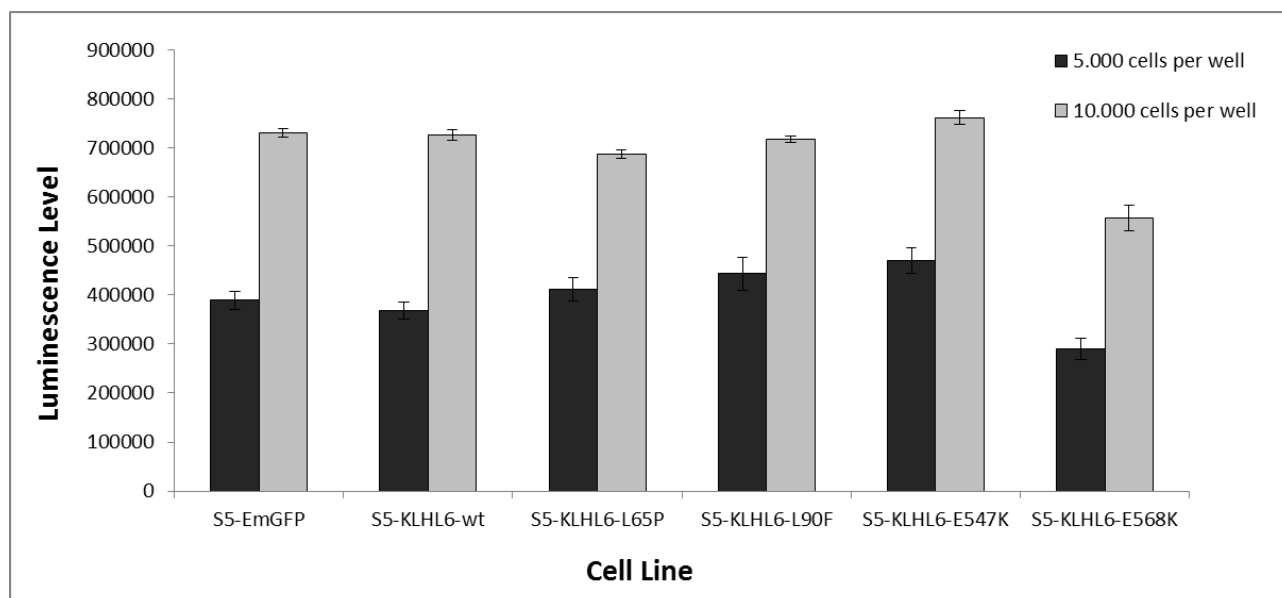


Figure 10. Average luminescence levels of all transduced SU-DHL-5 cell lines after a 72-hour incubation period. Aliquots of both 5,000 and 10,000 cells from each cell line were seeded into the wells of a 96-well plate. The proliferation rate was assessed using luminescence-based viability screening after 72 hours of incubation. The experiment was carried out in triplicate. The error bars represent the standard deviation between replicates.

4.2 Drug Sensitivity and Resistance Testing

To determine the consequences of KLHL6 mutations on drug response, I opted for an automated high-throughput drug response assay. To remove any detrimental effects on cell viability or proliferation caused by puromycin selection, the cells used for this assay were kept in puromycin-free medium for four passages beforehand.

To determine the optimal plating density of transduced SU-DHL-5 cells, I used the S5-EmGFP cell line. By choosing this cell line as a baseline for proliferation, the effects of transduction and KLHL6 overexpression on proliferation and viability were taken into account, since the S5-EmGFP cells were subjected to lentiviral transduction, but don't overexpress any form of KLHL6. The optimal density of transduced SU-DHL-5 cells in 384-well plates used for DSRT was determined by the DSRT team to be 2,500 cells per well.

The DSRT team carried out a drug screen using a panel of 528 drugs in five different concentrations in 10-fold dilutions covering a 10,000-fold concentration range. The screened cell lines were: S5-EmGFP, S5-KLHL6-wt, S5-KLHL6-L65P, S5-KLHL6-L90F, and S5-KLHL6-E547K. The raw data, drug response curves, and waterfall plots are available online^[117]. I used the resulting DSS values to calculate dDSS values. Since wild-type and mutant KLHL6 genes in transduced cell lines were overexpressed and had mutually similar expression levels of recombinant KLHL6 variants, the DSS values of the S5-KLHL6-wt cell line were chosen as the baseline for the comparison of mutant versus non-mutant cell line drug sensitivities. To determine if any significant mutation-independent effects of KLHL6 overexpression on drug sensitivity existed, I calculated dDSS values for the S5-KLHL6-wt cell line using the S5-EmGFP cell line as a baseline.

Out of the drugs tested, an average of 164 drugs (approximately 30 %) showed no discernable difference in effect between the control S5-KLHL6-wt cell line and the SU-DHL-5 cell lines transduced with KLHL6 mutants. Because of the absence of high dDSS values (e.g. between 10 and 40), which are usually produced and taken as significant in other studies that use the DSRT method, -2.0 and 2.0 were chosen here as arbitrary significance thresholds. On average, 63 % of all non-zero dDSS values of mutant cell lines fell into the range between -1.9 and 1.9 (below significance thresholds), and an average of 6 % (31.3) of absolute dDSS values of mutant cell lines were equal to or higher than 2.0 (above significance thresholds) (Table 8). Similarly, non-zero dDSS scores delineating the effects of KLHL6 overexpression on drug sensitivity were minor, and almost exclusively fell within the -1.9 to 1.9 range, with only 2,3% (11) of S5-KLHL6-wt dDSS values exceeding the significance thresholds (Table 8). When looking at the total number of drugs that produced significant dDSS values, the influence of KLHL6 overexpression on drug response was much weaker than that of mutations (Fig. 11).

Table 8. Distribution of DSRT results (dDSS values). Differential DSS values for the S5-KLHL6-wt cell line were calculated by subtracting the DSS value of the S5-EmGFP cell line from the DSS values of the S5-KLHL6-wt cell line for the same drug, and dDSS values for mutant-expressing cell lines were calculated by subtracting the DSS value of the S5-KLHL6-wt cell line from the DSS value of a mutant-expressing cell line for the same drug. DSRT - drug sensitivity and resistance testing; DSS - drug sensitivity score.

Cell Line	Number (Percentage) of dDSS Values Within a Value Range				
	≤ -2.0	[-1.9, 0.0>	0.0	<0.0, 1.9]	≥ 2.0
S5-KLHL6-wt	7 (1.3 %)	210 (40.0 %)	176 (33.3 %)	131 (24.8 %)	4 (1.0 %)
S5-KLHL6-L65P	12 (2.3 %)	187 (35.4 %)	168 (31.8 %)	147 (27.8 %)	14 (2.7 %)
S5-KLHL6-L90F	10 (1.9 %)	167 (31.6 %)	163 (30.9 %)	169 (32.0 %)	19 (3.6 %)
S5-KLHL6-E547K	6 (1.1 %)	116 (22.0 %)	162 (30.1 %)	211 (40.0 %)	33 (6.3 %)
Average Number of dDSS Values of Mutants Within a Range	9.3	156.7	164.3	175.7	22
Percentage of Total dDSS Values of Mutants Within a Range	1.8 %	29.7 %	31.1 %	33.3 %	4.2 %

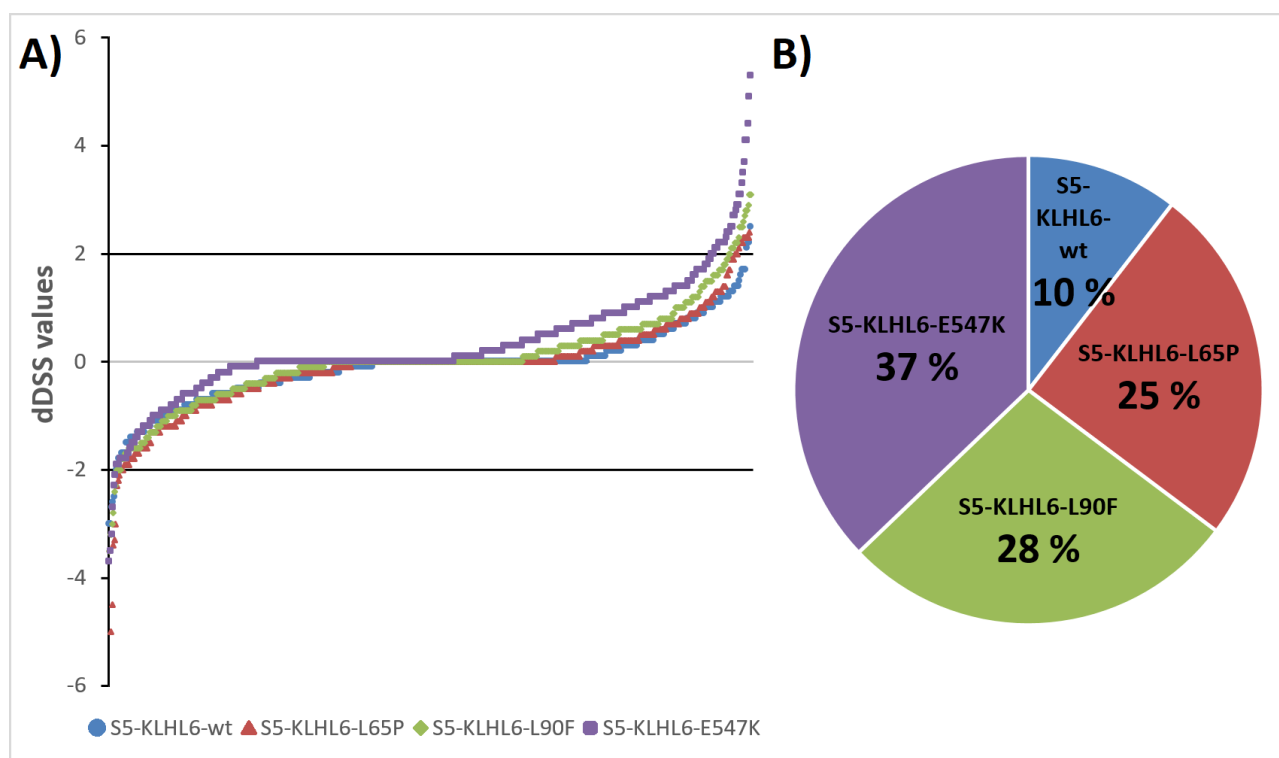


Figure 11. A) Graphical representation of the dDSS values for each cell line produced by all tested drugs. The dDSS values were ordered from most negative to most positive for each cell line. The outlier dDSS value of Ixabepilone (S5-KLHL6-L65P) (-9.6) is not shown. B) Share of total significant dDSS values produced by each cell line. dDSS - differential drug sensitivity score.

Taking the entirety of the DSRT results into account, the dDSS value of -9.6 resulting from Ixabepilone treatment of S5-KLHL6-L65P cells (Fig. 12) was by far the most prominent, being almost twice as high as the next highest dDSS value of 5.3 when considering the values as absolutes (Fig. 13). Several drugs that produced the top 20 and bottom 20 dDSS values for each cell line had similar mechanisms/targets. The 1st, 3rd, and 9th highest sensitivity increases observed for the S5-KLHL6-L65P cell line were produced by PI3K inhibitors: Idelalisib, GDC-0084 and Duvelisib, with dDSS values of 2.4, 2.3, and 2.2, respectively. The 5th and 6th highest resistance increases (or sensitivity decreases) for the same cell line, with dDSS values of -3.3 and -3.0, respectively, were produced by AKT inhibitors: Triciribine and MK-2206, complementing the observation of the cell line's increased sensitivity to PI3K inhibition. The 2nd, 6th, and 11th highest increases in sensitivity for the S5-KLHL6-L90F cell line were produced by anti-apoptotic compounds: Sabutoclax, Idasanutlin and PAC-1, with dDSS values of 3.1, 2.7, and 2.3, respectively. No repeatedly-targeted pathways were noted among the top dDSS values for the S5-KLHL6-E547K cell line (Fig. 13) or among the dDSS values above the significance threshold for the S5-KLHL6-wt cell line.

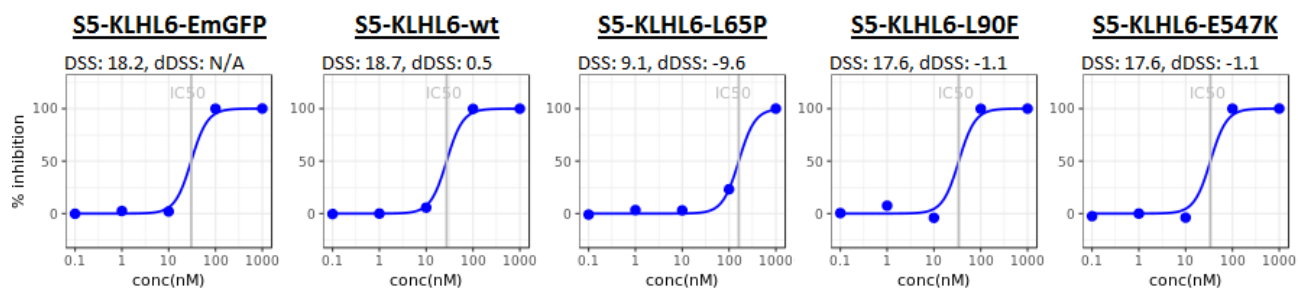


Figure 12. Dose response curves of transduced SU-DHL-5 cell lines treated with 10-fold dilutions of Ixabepilone covering a 10,000-fold concentration range. Differential DSS values for mutant cell lines were calculated by subtracting the DSS value of the S5-KLHL6-wt cell line from the DSS values of cell lines expressing mutant variants for the same drug, and dDSS values for the S5-EmGFP cell line were calculated by subtracting the DSS values of the S5-EmGFP cell line from the S5-EmGFP cell line's DSS values for the same drug. DSS - drug sensitivity score; dDSS - differential drug sensitivity score.

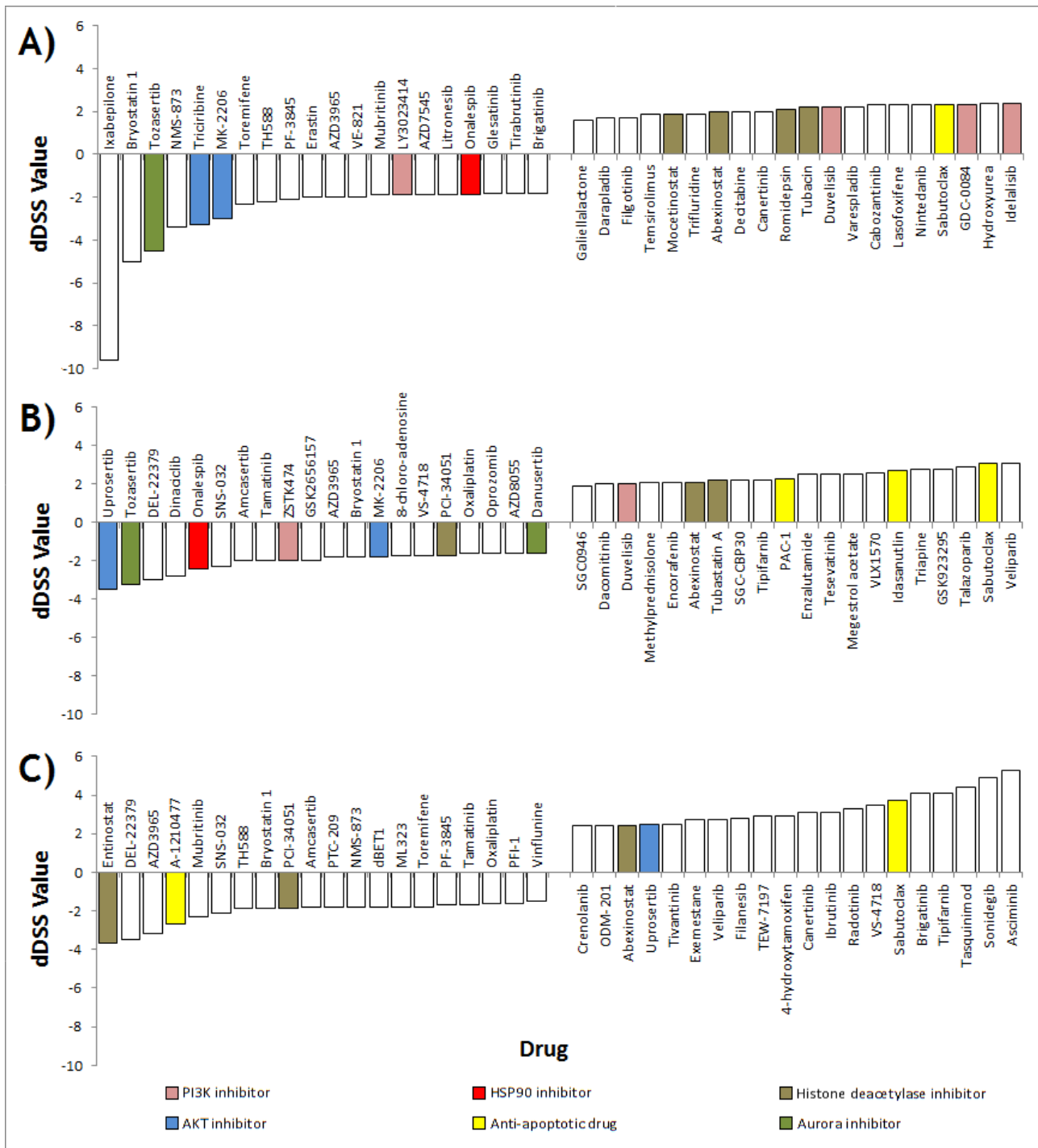


Figure 13. Drugs with the largest differences in effect between the S5-KLHL6-L65P cell line (A), S5-KLHL6-L90F cell line (B), or S5-KLHL6-E547K cell line (C) and the control S5-KLHL6-wt cell line, sorted by dDSS value. Columns representing drugs that share the same select target are highlighted in the same color: pink - PI3K inhibitors, blue - AKT inhibitors, red - HSP90 inhibitors, yellow - anti-apoptotic drugs, brown - histone deacetylase inhibitors, green - Aurora inhibitors, white - variety of targets. dDSS - differential drug sensitivity score.

4.3 Verification of DSRT Results

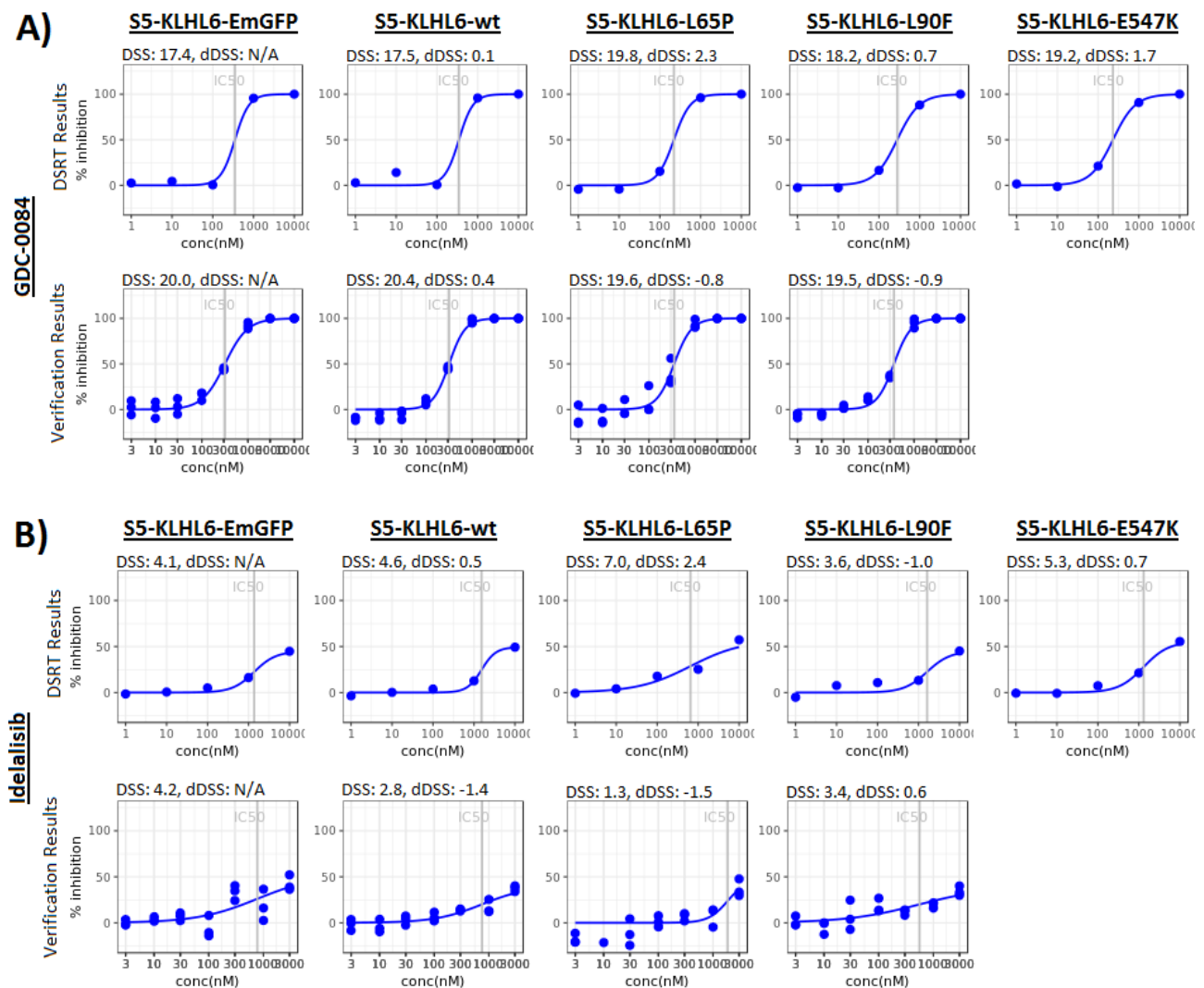
Before proceeding with further in-depth testing based on dDSS values, I attempted to verify the most prominent results in order to rule out any false positives, especially because no replicates were used in the DSRT.

To confirm the DSRT results, all cell lines used in DSRT, except the S5-KLHL6-E547K cell line, were plated onto 96-well plates. The S5-KLHL6-E547K cell line was omitted from verification due to a lack of promising drug screening results. Drugs the plated cells were treated with were chosen from the top dDSS scores of the S5-KLHL6-L65P and S5-KLHL6-L90F cell lines. The chosen drugs targeted a variety of cellular pathways, with emphasis on the PI3K/AKT pathway. Drug responses were quantified using a luminescence assay after three days of drug treatment.

The effects of the KLHL6-L65P and KLHL6-L90F mutations on the response to GDC-0084, a PI3K inhibitor, between DSRT and verification results were in disagreement. The DSRT results indicated increased sensitivity of the mutant-expressing cells to the drug, while the results of the verification test showed a decrease (Fig. 14-A). The same kind of discrepancy between the results of the two experiments was observed for the response to Idelalisib, another PI3K inhibitor, where increases and decreases of sensitivity to the drug were reversed (Fig. 14-B). Verification of the responses to Onalespib, an HSP90 inhibitor, validated the small decrease in sensitivity of the S5-KLHL6-L65P cells to the drug compared to S5-KLHL6-wt cells, though at a much lower degree than in DSRT results. However, no change in sensitivity to Onalespib induced by the KLHL6-L90F mutation was shown by verification results, contradictory to the slight decrease in sensitivity demonstrated by DSRT (Fig. 14-C). Both attempts at verifying the effects the KLHL6-L65P and KLHL6-L90F mutations had on the cells' response to Ixabepilone resulted in mutually similar outcomes, which were antithetical to the outcome of DSRT. The dDSS values of the S5-KLHL6-L65P cell line calculated from verification results were far lower than the value of -9.6 produced by DSRT, reaching a maximum of only -0.6. Additionally, the drug response curves modeled using the data points from the verification experiments indicated a dose-dependent increase in cell death comparable to the one resulting from DSRT, but at nearly tenfold lower drug concentrations (Fig. 14-D). Effects of KLHL6 overexpression on the cells' sensitivities to the drugs used in verification were both negligible and discordant between DSRT and verification (Fig. 14: A-D).

To estimate whether these discrepancies were merely a result of variability, a more direct comparison was made between the effects of the same concentrations of drugs used in both DSRT and verification experiments on cell viability. Error bars were constructed using the triplicates from the verification experiments (Fig. 15). Most of the DSRT results fell either near or within the error bars.

My second attempt at verification of the large increase of the resistance of S5-KLHL6-L65P cells to Ixabepilone failed to replicate DSRT results, and resulted in a nearly-identical outcome to the first verification attempt. Because of this, combined with conflicting results obtained from other verification experiments, the effects of KLHL6 mutations on drug response were deemed insignificant, and no further experimentation was performed on the mutant cell lines.



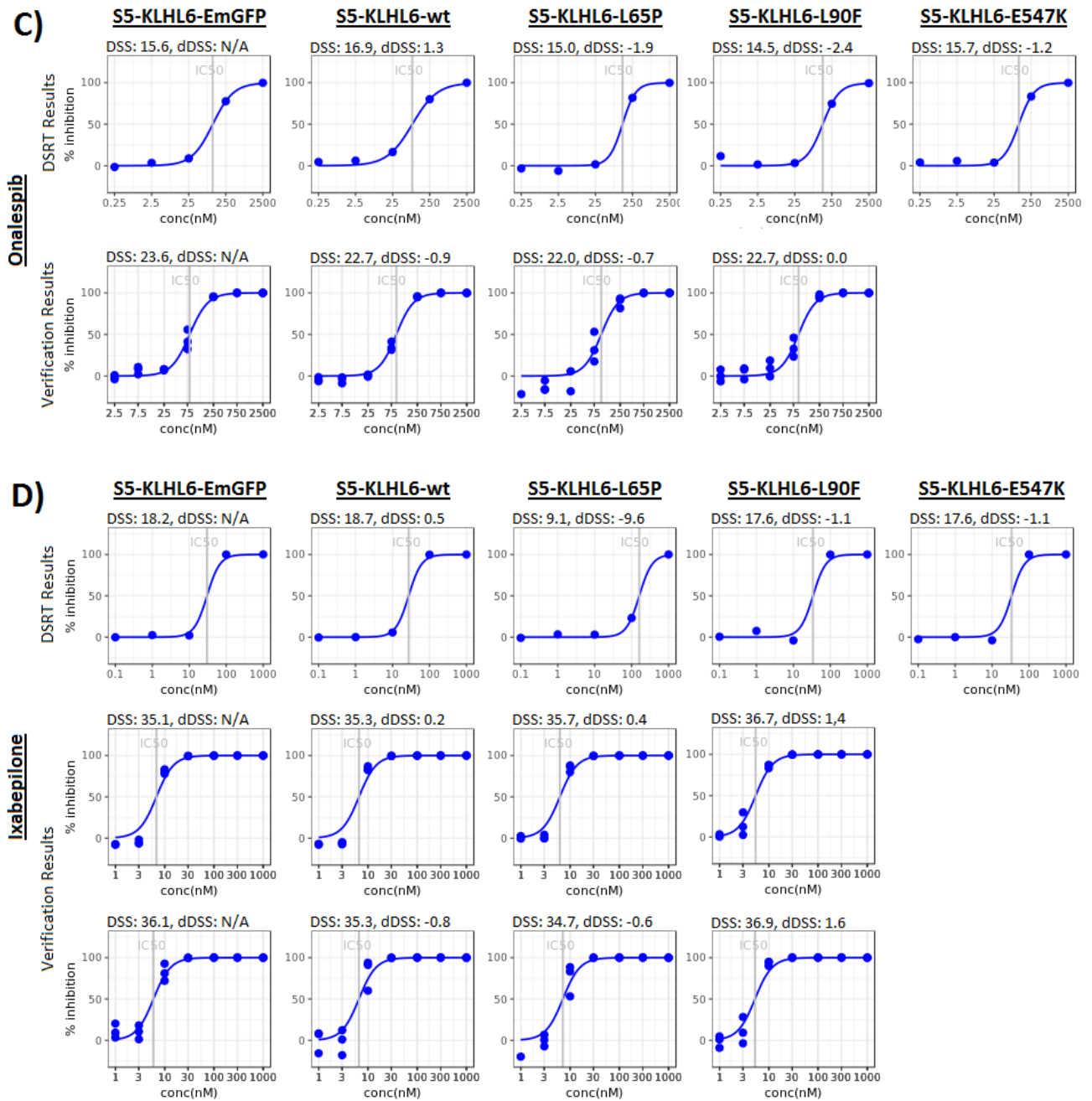
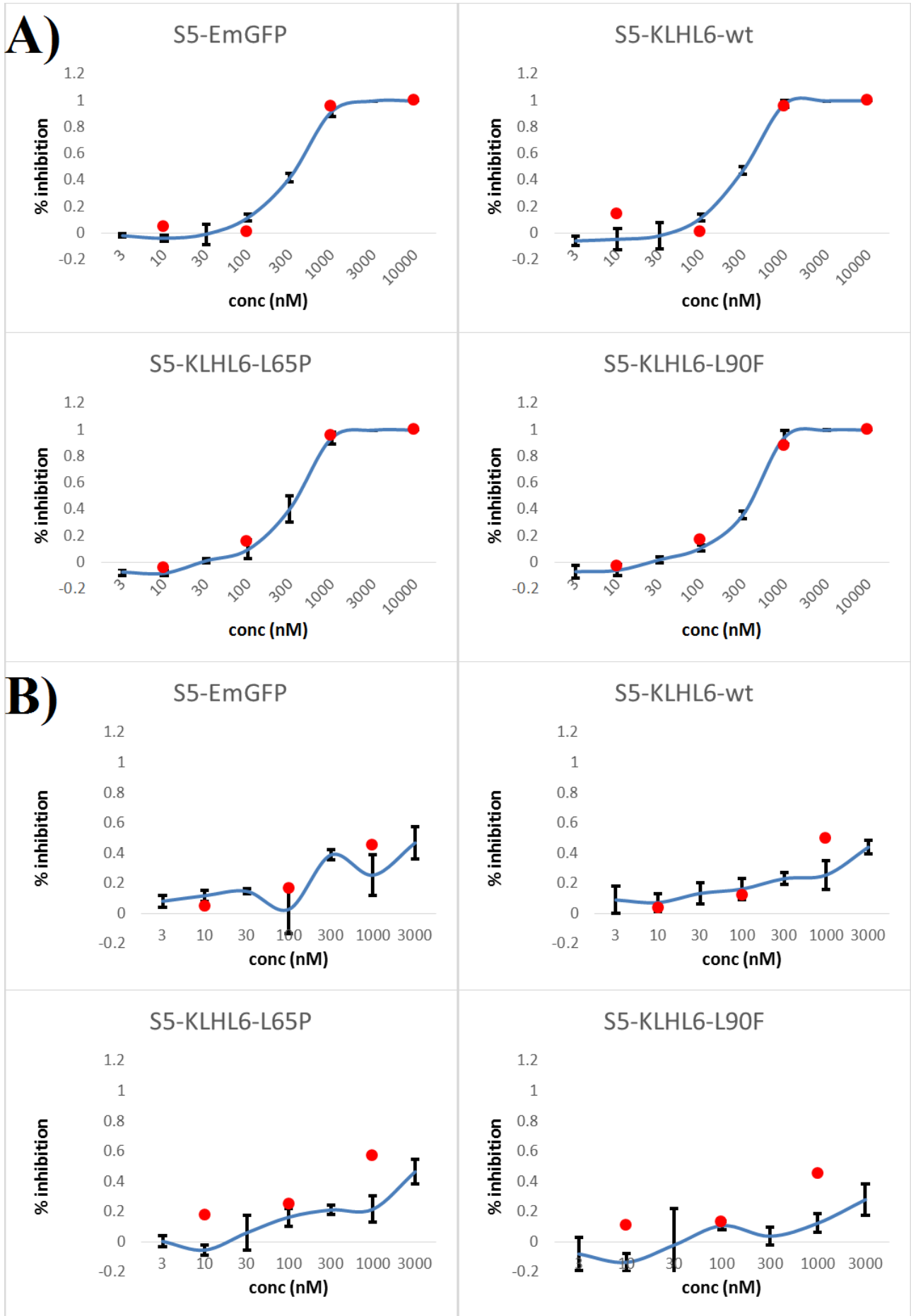
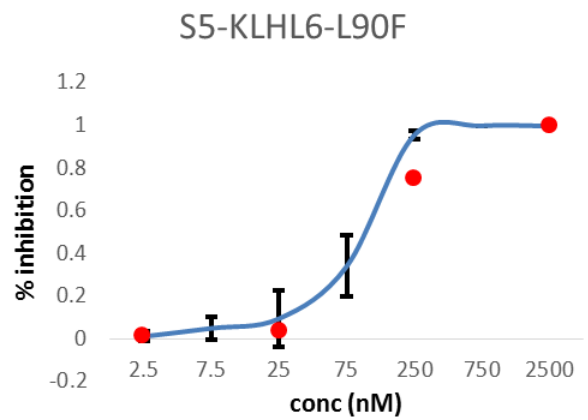
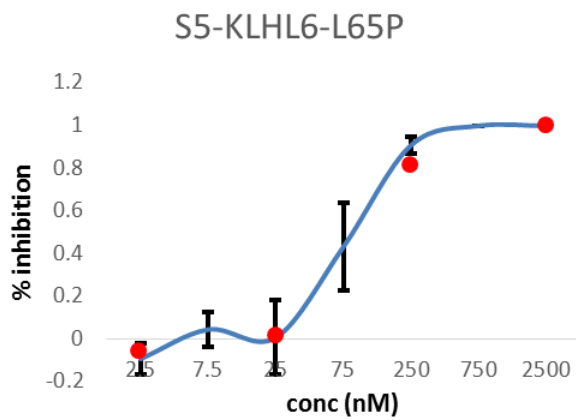
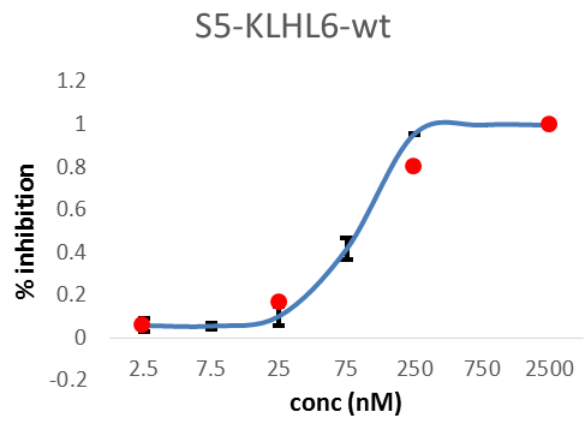
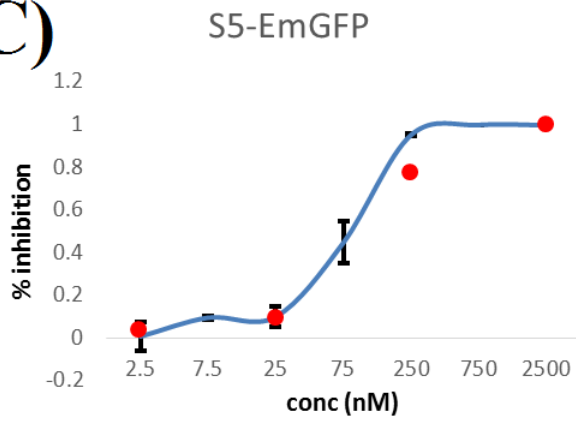
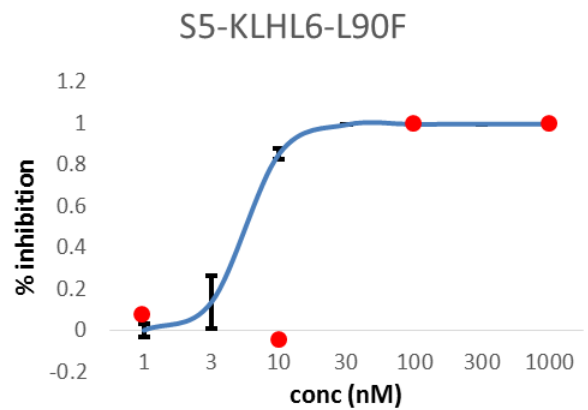
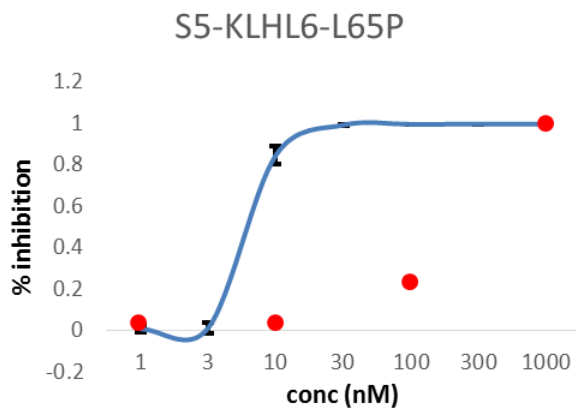
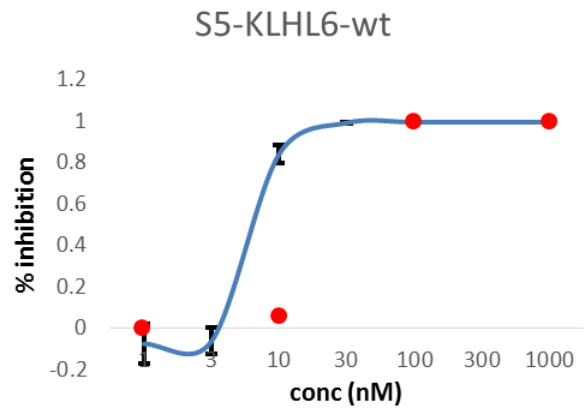
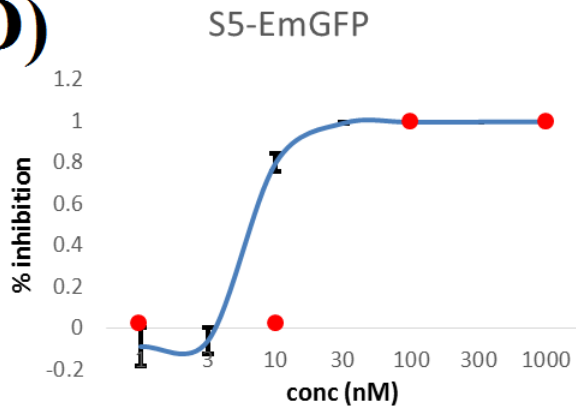


Figure 14. Side-by-side comparison of drug response curves modeled using data from DSRT and verification experiments. The drugs used in verification experiments are: (A) GDC-0084, (B) Idelalisib, (C) Onalespib, and (D) Ixabepilone. Differential DSS values for mutant cell lines were calculated by subtracting the DSS value of the S5-KLHL6-wt cell line from the DSS values of cell lines expressing mutant variants for the same drug, and dDSS values for the S5-EmGFP cell line were calculated by subtracting the DSS values of the S5-EmGFP cell line's DSS values for the same drug. DSS - drug sensitivity score.



C)**D)**

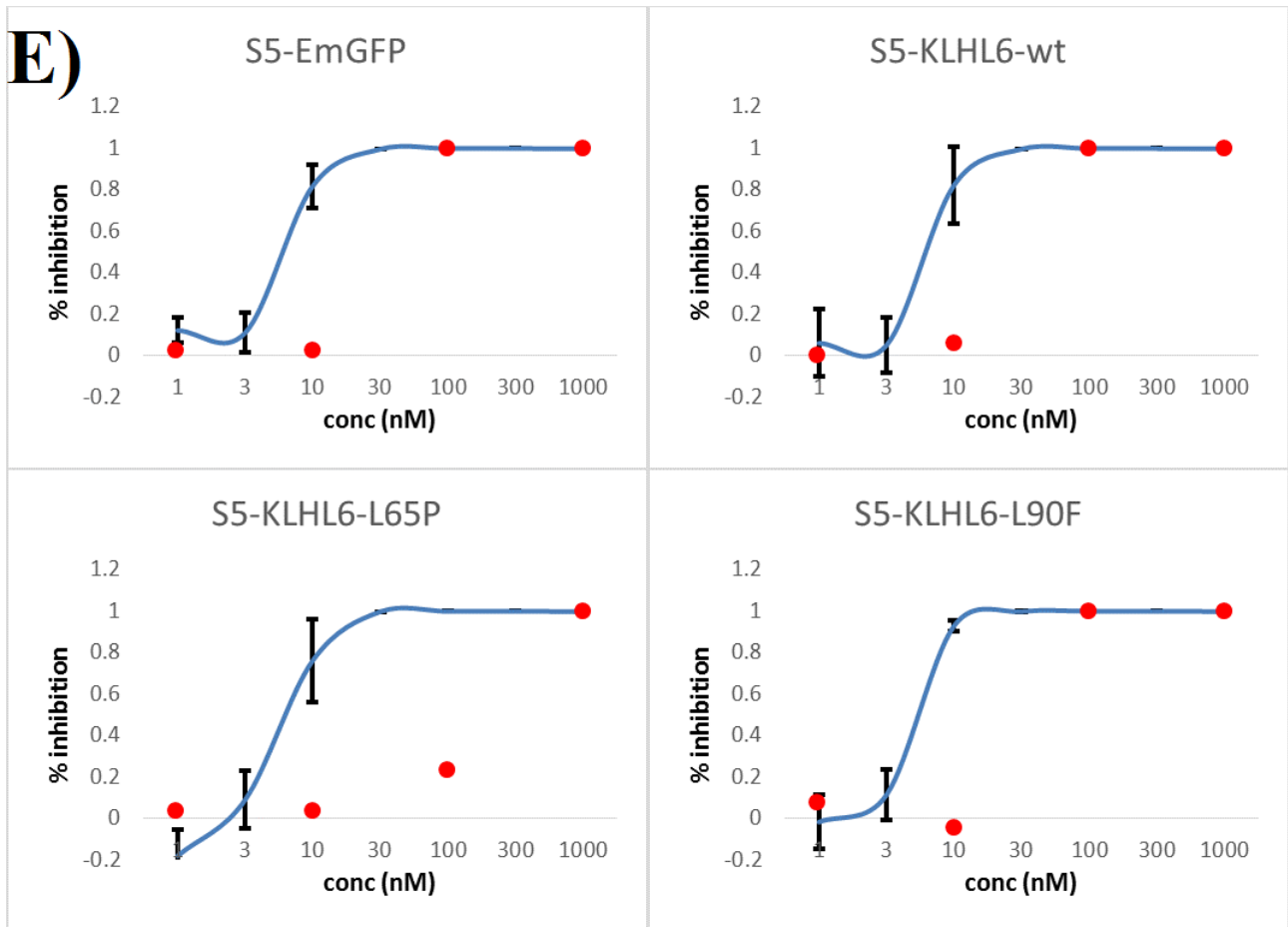


Figure 15. Drug response curves comparing the inhibitory effects of drugs in concentrations used both for DSRT and verification experiments. Drug response curves and error bars were constructed from the results of the verification experiments. Red dots represent cell growth inhibition values resulting from DSRT. A) GDC-0084; B) Idelalisib; C) Onalespib; D) Ixabepilone - verification attempt 1; E) Ixabepilone - verification attempt 2. DSRT - drug sensitivity and resistance testing.

5. DISCUSSION

With this study, I aimed to elucidate the effects of the most common KLHL6 mutations in DLBCL on drug response, enriching the very limited amount of knowledge attained about the protein thus far, and possibly opening an avenue towards targeted DLBCL therapy.

5.1 Studied KLHL6 Mutations Might Not Affect Drug Response

The DSRT platform has previously been successfully employed by Pemovska et al. in the identification of actionable drug vulnerabilities of chemorefractory AML cases^[119], as well as in discerning Axitinib as a selective inhibitor of the BCR-ABL1 fusion protein carrying a T315I missense mutation^[120]. Using the same platform and utilizing more than twice the number of drugs, I observed no significant changes in drug response linked to the studied KLHL6 mutations or overexpression.

Although the DSRT results showed only minor changes in drug response, the effect of KLHL6 mutants on drug sensitivity was slightly greater than that of KLHL6 overexpression. This led me to perform an in-depth analysis of the top scores for each tested cell line in order to investigate if any cellular pathways were present in multiple instances. Although a few pathways were found to be repeatedly affected by changes in susceptibility to drugs, the repeated hits to the PI3K/AKT pathway produced by the S5-KLHL6-L65P cell line stood out the most. I decided to focus my verification efforts on these results because the dysregulation of the PI3K/AKT pathway has previously been shown to preferentially affect the GCB type of DLBCL^[33,34], which my model cell line had been classified as^[115]. Onalespib was also used in the verification experiment on the grounds of the sensitivities of both BTB-domain mutants to it being affected in a similar way. Although the same logic could have been used in favor of the verification of the results of Tozasertib, its drug response curves were highly irregular^[117], which deterred me from attempting to verify its effects. Lastly, the effects of Ixabepilone on the S5-KLHL6-L65P cell line were chosen for verification simply due to the magnitude of the observed change in the cells' sensitivity to the drug.

Unfortunately, almost none of the dDSS values produced by verification experiments matched the original DSRT results. Drug sensitivity increases of cells resulting from DSRT almost exclusively manifested as decreases in the verification experiment and vice versa. I attributed this occurrence to the combination of the absence of replicates in the DSRT, and low dDSS values produced both by DSRT and verification experiments. My reasoning is that the differences in viability decreases caused by the same concentrations of the same drugs from both sets of experimental data are most likely within each other's error bars, with the error bars of the DSRT results being imaginary since no replicates were used. This would attribute the observed contradiction of results between DSRT and verification experiments to the variability of the already small dDSS values.

The fact that the drugs used in DSRT were printed onto the plates and kept in a dry environment, and the drugs used for verification were dissolved directly into the cell medium could be a factor contributing to the discrepancy in the IC₅₀ values observed between the results of DSRT and verification experiments involving Ixabepilone. Although no data is available on the stability of Ixabepilone in a dry environment, the timespan between drug printing and DSRT was presumably too short for a significant degree of Ixabepilone degradation to occur. My assumption is that the observed large difference in its IC₅₀ values between experiments is due to Ixabepilone being difficult to re-dissolve after drying, especially since no mixing or shaking was used to assist drug dissolution during DSRT.

Altogether, the outcomes of these experiments provide data which indicates that the hypothesis that KLHL6 mutations influence drug sensitivity in DLBCL was not correct. Additionally, due to no consistent modulation of any cellular pathways by the investigated mutations being evident, I wasn't able to narrow down the possible functions KLHL6 might perform in either DLBCL or B-lymphocytes.

5.2 Possible Influences on the Outcome of the Study

In the studies of Pemovska et al., relatively large numbers of tested drugs have produced dDSS values larger than 10, with multiple dDSSs reaching values of between 30 and 40, thus making the distinction of mutant-/cancer-selective drugs clear^[119,120]. In their AML study, they have used a dDSS significance cutoff of $10^{[119]}$. This cutoff has also been used in other later studies in which the DSRT platform has successfully been utilized for the discovery of cancer-selective drugs^[121-123]. Compared to these studies, my experiments produced almost no changes in drug sensitivity which could be considered significant, with only three dDSSs out of a total of 2,112 reaching values equal to or higher than 5 and none of them surpassing a value of 10. In contrast to my study, the aforementioned research groups have analyzed changes in drug sensitivities either caused by well-studied mutations^[120], or between subjects and controls possessing a much greater degree of genetic variation (e.g. tumor cells and normal, healthy cells)^[119,121-123], which would account for the greater numbers of prominent results their screens had produced. The scarcity of high dDSS values resulting from my implementation of the DSRT platform most likely arose as a consequence of the fact that the subject was a set of never before studied single-nucleotide missense mutations. This opens up the possibility that said mutations might not have any consequences on the functions of KLHL6 at all. This outlook on the matter is supported by the recent findings of Bertocci et al. in which they have postulated that KLHL6 mutations might not possess any oncogenic potential, but are simply a common off-target of the somatic hypermutation process^[101]. Another viable explanation of the experimental results is that, although high expression levels of KLHL6 variants in transduced cell lines were observed, the mutations themselves could have either been inactivating, making the endogenous KLHL6 protein the sole functional variant in transduced cells, or could have only slightly altered the topology of the protein in such a way that the mutant protein's strong overexpression compensated for any decrease in its functionality. Lastly, because cultured cells were used, the influence of the tumor microenvironment on cell functions was completely abolished, which could have also had an impact on drug response.

5.3 Future Prospects

The outcome of this study should neither discourage future experimentation focusing on KLHL6 mutants, nor discredit the DSRT platform, but serve as stepping stone towards an improved model of DLBCL and refined application of the methodology. Due to its importance in B-lymphocyte ontogeny^[99,101], and the relatively high frequency of its mutated variants present in lymphoid malignancies^[30,102-110], KLHL6 inarguably deserves further research devoted to its structure, cellular functions and functional consequences of its mutations. A repeat of this study could be done using a DLBCL cell line whose endogenous *KLHL6* gene is directly replaced by a mutated variant. This would eliminate both the influences of the endogenous gene and of the mutant's overexpression. Perhaps a different cell line, whose survival depends on a functional KLHL6 protein or one of its mutant variants, may be able to better outline the roles of KLHL6 in B-lymphocytes or of its mutant variants in DLBCL, respectively. An untagged protein should be used in order to have as few influences on KLHL6 function as possible. A different kind of study, using transgenic mice whose endogenous KLHL6 either carries a mutation in the BTB or kelch domain, or whose BTB or kelch domain is deleted, may be able to shed light on the importance of each domain in the maturation process of B-lymphocytes. More information about KLHL6, more specifically its interaction partners, may also be collected by co-immunoprecipitation studies. By using antibodies specific for a certain domain of KLHL6, either of the remaining domains could be deleted. In the absence of domain-specific antibodies, this could also be accomplished by using molecular tags and tag-specific antibodies. Protein interactions the deleted domain mediates could be identified by comparison of results between co-immunoprecipitation experiments using wild-type and trimmed KLHL6 proteins. By doing KLHL6 co-immunoprecipitation experiments on protein extracts from B-lymphocytes undergoing different stages of maturation, the elucidation of the role of KLHL6 in B-lymphocyte development might be possible.

6. CONCLUSION

Compared to other methods used for the identification of the functional consequences of a missense mutation, such as co-immunoprecipitation or analysis of enzymatic activity, DSRT is an approach much less focused on previously-known protein characteristics and offers the possibility of detection of unexpected effects of protein mutations. In my case, high-throughput drug screening wasn't able to produce any definitive results outlining functional changes induced by the most common KLHL6 mutations. This raises doubts both about the significance of KLHL6 and its mutations in DLBCL, and also about the utility of the drug screening method itself in studies of previously-uninvestigated missense mutations using model cell lines.

7. REFERENCES

1. Perry AM, Diebold J, Nathwani BN, MacLennan KA, Muller-Hermelink HK, Bast M, et al. Non-Hodgkin lymphoma in the developing world: review of 4539 cases from the International Non-Hodgkin Lymphoma Classification Project. *Haematologica*. 2016;101(10):1244-50.
2. Alizadeh AA, Eisen MB, Davis RE, Ma C, Lossos IS, Rosenwald A, et al. Distinct types of diffuse large B-cell lymphoma identified by gene expression profiling. *Nature*. 2000;403(6769):503-11.
3. Swerdlow SH, Campo E, Pileri SA, Harris NL, Stein H, Siebert R, et al. The 2016 revision of the World Health Organization classification of lymphoid neoplasms. *Blood*. 2016;127(20):2375-90.
4. Swerdlow SH, International Agency for Research on Cancer. WHO Classification of tumors of haematopoietic and lymphoid tissues. 4 ed. Lyon: IARC Press; 2008. 439 p.
5. Shaffer AL, 3rd, Young RM, Staudt LM. Pathogenesis of human B cell lymphomas. *Annu Rev Immunol*. 2012;30:565-610.
6. Allen CDC, Okada T, Cyster JG. Germinal-center organization and cellular dynamics. *Immunity*. 2007;27(2):190-202.
7. Li S, Young KH, Medeiros LJ. Diffuse large B-cell lymphoma. *Pathology*. 2018;50(1):74-87.
8. Hans CP, Weisenburger DD, Greiner TC, Gascoyne RD, Delabie J, Ott G, et al. Confirmation of the molecular classification of diffuse large B-cell lymphoma by immunohistochemistry using a tissue microarray. *Blood*. 2004;103(1):275-82.
9. Rosenwald A, Wright G, Chan WC, Connors JM, Campo E, Fisher RI, et al. The use of molecular profiling to predict survival after chemotherapy for diffuse large-B-cell lymphoma. *New Engl J Med*. 2002;346(25):1937-47.

10. Arber DA, Weiss LM. CD10 - A review. *Appl Immunohistochem*. 1997;5(3):125-40.
11. Dogan A, Bagdi E, Munson P, Isaacson PG. CD10 and BCL-6 expression in paraffin sections of normal lymphoid tissue and B-cell lymphomas. *Am J Surg Pathol*. 2000;24(6):846-52.
12. Cattoretti G, Chang CC, Cechova K, Zhang JD, Ye BH, Falini B, et al. Bcl-6 Protein Is Expressed in Germinal-Center B-Cells. *Blood*. 1995;86(1):45-53.
13. De Silva NS, Klein U. Dynamics of B cells in germinal centres. *Nat Rev Immunol*. 2015;15(3):137-48.
14. Chang CC, Ye BH, Chaganti RSK, DallaFavera R. BCL-6, a POZ/zinc-finger protein, is a sequence-specific transcriptional repressor. *P Natl Acad Sci USA*. 1996;93(14):6947-52.
15. Eisenbeis CF, Singh H, Storb U. Pip, a Novel Irf Family Member, Is a Lymphoid-Specific, Pu.1-Dependent Transcriptional Activator. *Gene Dev*. 1995;9(11):1377-87.
16. Falini B, Fizzotti M, Pucciarini A, Bigerna B, Marafioti T, Gambacorta M, et al. A monoclonal antibody (MUM1p) detects expression of the MUM1/IRF4 protein in a subset of germinal center B cells, plasma cells, and activated T cells. *Blood*. 2000;95(6):2084-92.
17. Meyer PN, Fu K, Greiner TC, Smith LM, Delabie J, Gascoyne RD, et al. Immunohistochemical Methods for Predicting Cell of Origin and Survival in Patients With Diffuse Large B-Cell Lymphoma Treated With Rituximab. *J Clin Oncol*. 2011;29(2):200-7.
18. Choi WWL, Weisenburger DD, Greiner TC, Piris MA, Banham AH, Delabie J, et al. A New Immunostain Algorithm Classifies Diffuse Large B-Cell Lymphoma into Molecular Subtypes with High Accuracy. *Clin Cancer Res*. 2009;15(17):5494-502.
19. Muris JJ, Meijer CJ, Vos W, van Krieken JH, Jiwa NM, Ossenkoppele GJ, et al. Immunohistochemical profiling based on Bcl-2, CD10 and MUM1 expression improves risk stratification in patients with primary nodal diffuse large B cell lymphoma. *J Pathol*. 2006;208(5):714-23.

20. Scott DW, Wright GW, Williams PM, Lih CJ, Walsh W, Jaffe ES, et al. Determining cell-of-origin subtypes of diffuse large B-cell lymphoma using gene expression in formalin-fixed paraffin-embedded tissue. *Blood*. 2014;123(8):1214-7.
21. Geiss GK, Bumgarner RE, Birditt B, Dahl T, Dowidar N, Dunaway DL, et al. Direct multiplexed measurement of gene expression with color-coded probe pairs. *Nat Biotechnol*. 2008;26(3):317-25.
22. Carbone PP, Kaplan HS, Musshoff K, Smithers DW, Tubiana M. Report of the Committee on Hodgkin's Disease Staging Classification. *Cancer Res*. 1971;31(11):1860-1.
23. Lister TA, Crowther D, Sutcliffe SB, Glatstein E, Canellos GP, Young RC, et al. Report of a Committee Convened to Discuss the Evaluation and Staging of Patients with Hodgkins-Disease - Cotswolds Meeting. *J Clin Oncol*. 1989;7(11):1630-6.
24. Rosenberg SA. Validity of the Ann Arbor staging classification for the non-Hodgkin's lymphomas. *Cancer Treat Rep*. 1977;61(6):1023-7.
25. The International Non-Hodgkin's Lymphoma Prognostic Factors Project. A predictive model for aggressive non-Hodgkin's lymphoma. *N Engl J Med*. 1993;329(14):987-94.
26. Sehn LH, Berry B, Chhanabhai M, Fitzgerald C, Gill K, Hoskins P, et al. The revised International Prognostic Index (R-IPI) is a better predictor of outcome than the standard IPI for patients with diffuse large B-cell lymphoma treated with R-CHOP. *Blood*. 2007;109(5):1857-61.
27. Ngo L, Hee SW, Lim LC, Tao M, Quek R, Yap SP, et al. Prognostic factors in patients with diffuse large B cell lymphoma: Before and after the introduction of rituximab. *Leukemia Lymphoma*. 2008;49(3):462-9.
28. Zhou Z, Sehn LH, Rademaker AW, Gordon LI, LaCasce AS, Crosby-Thompson A, et al. An enhanced International Prognostic Index (NCCN-IPI) for patients with diffuse large B-cell lymphoma treated in the rituximab era. *Blood*. 2014;123(6):837-42.
29. Kubuschok B, Held G, Pfreundschuh M. Management of diffuse large B-cell lymphoma (DLBCL). *Cancer treatment and research*. 2015;165:271-88.

30. Schmitz R, Wright GW, Huang DW, Johnson CA, Phelan JD, Wang JQ, et al. Genetics and Pathogenesis of Diffuse Large B-Cell Lymphoma. *New Engl J Med*. 2018;378(15):1396-407.
31. Lenz G, Wright G, Dave SS, Xiao W, Powell J, Zhao H, et al. Stromal Gene Signatures in Large-B-Cell Lymphomas. *New Engl J Med*. 2008;359(22):2313-23.
32. Morin RD, Mungall K, Pleasance E, Mungall AJ, Goya R, Huff RD, et al. Mutational and structural analysis of diffuse large B-cell lymphoma using whole-genome sequencing. *Blood*. 2013;122(7):1256-65.
33. Karube K, Enjuanes A, Dlouhy I, Jares P, Martin-Garcia D, Nadeu F, et al. Integrating genomic alterations in diffuse large B-cell lymphoma identifies new relevant pathways and potential therapeutic targets. *Leukemia*. 2018;32(3):675-84.
34. Pfeifer M, Grau M, Lenze D, Wenzel SS, Wolf A, Wollert-Wulf B, et al. PTEN loss defines a PI3K/AKT pathway-dependent germinal center subtype of diffuse large B-cell lymphoma. *P Natl Acad Sci USA*. 2013;110(30):12420-5.
35. Pasqualucci L, Dominguez-Sola D, Chiarenza A, Fabbri G, Grunn A, Trifonov V, et al. Inactivating mutations of acetyltransferase genes in B-cell lymphoma. *Nature*. 2011;471(7337):189-95.
36. Morin RD, Johnson NA, Severson TM, Mungall AJ, An JH, Goya R, et al. Somatic mutations altering EZH2 (Tyr641) in follicular and diffuse large B-cell lymphomas of germinal-center origin. *Nat Genet*. 2010;42(2):181-5.
37. Morin RD, Mendez-Lago M, Mungall AJ, Goya R, Mungall KL, Corbett RD, et al. Frequent mutation of histone-modifying genes in non-Hodgkin lymphoma. *Nature*. 2011;476(7360):298-303.
38. Chun J, Hla T, Lynch KR, Spiegel S, Moolenaar WH. International Union of Basic and Clinical Pharmacology. LXXVIII. Lysophospholipid Receptor Nomenclature. *Pharmacol Rev*. 2010;62(4):579-87.

39. Green JA, Suzuki K, Cho B, Willison LD, Palmer D, Allen CD, et al. The sphingosine 1-phosphate receptor S1P(2) maintains the homeostasis of germinal center B cells and promotes niche confinement. *Nat Immunol.* 2011;12(7):672-80.
40. Schwab SR, Cyster JG. Finding a way out: lymphocyte egress from lymphoid organs. *Nat Immunol.* 2007;8(12):1295-301.
41. West KA, Castillo SS, Dennis PA. Activation of the PI3K/Akt pathway and chemotherapeutic resistance. *Drug Resist Update.* 2002;5(6):234-48.
42. Jin QH, Yu LR, Wang LF, Zhang ZJ, Kasper LH, Lee JE, et al. Distinct roles of GCN5/PCAF-mediated H3K9ac and CBP/p300-mediated H3K18/27ac in nuclear receptor transactivation. *Embo J.* 2011;30(2):249-62.
43. Lill NL, Grossman SR, Ginsberg D, DeCaprio J, Livingston DM. Binding and modulation of p53 by p300/CBP coactivators. *Nature.* 1997;387(6635):823-7.
44. Tang Y, Zhao WH, Chen Y, Zhao YM, Gu W. Acetylation is indispensable for p53 activation. *Cell.* 2008;133(4):612-26.
45. Shaffer AL, Yu X, He YS, Boldrick J, Chan EP, Staudt LM. BCL-6 represses genes that function in lymphocyte differentiation, inflammation, and cell cycle control. *Immunity.* 2000;13(2):199-212.
46. Bereshchenko OR, Gu W, Dalla-Favera R. Acetylation inactivates the transcriptional repressor BCL6. *Nat Genet.* 2002;32(4):606-13.
47. Gossett LA, Kelvin DJ, Sternberg EA, Olson EN. A New Myocyte-Specific Enhancer-Binding Factor That Recognizes a Conserved Element Associated with Multiple Muscle-Specific Genes. *Mol Cell Biol.* 1989;9(11):5022-33.
48. Sartorelli V, Huang J, Hamamori Y, Kedes L. Molecular mechanisms of myogenic coactivation by p300: Direct interaction with the activation domain of MyoD and with the MADS box of MEF2C. *Mol Cell Biol.* 1997;17(2):1010-26.

49. Youn HD, Sun L, Prywes R, Liu JO. Apoptosis of T cells mediated by Ca²⁺-induced release of the transcription factor MEF2. *Science*. 1999;286(5440):790-3.
50. Youn HD, Liu JO. Cabin1 represses MEF2-dependent Nur77 expression and T cell apoptosis by controlling association of histone deacetylases and acetylases with MEF2. *Immunity*. 2000;13(1):85-94.
51. Ying CY, Dominguez-Sola D, Fabi M, Lorenz IC, Hussein S, Bansal M, et al. MEF2B mutations lead to deregulated expression of the oncogene BCL6 in diffuse large B cell lymphoma. *Nat Immunol*. 2013;14(10):1084-92.
52. Kirmizis A, Bartley SM, Kuzmichev A, Margueron R, Reinberg D, Green R, et al. Silencing of human polycomb target genes is associated with methylation of histone H3 Lys 27. *Gene Dev*. 2004;18(13):1592-605.
53. Yap DB, Chu J, Berg T, Schapira M, Cheng SWG, Moradian A, et al. Somatic mutations at EZH2 Y641 act dominantly through a mechanism of selectively altered PRC2 catalytic activity, to increase H3K27 trimethylation. *Blood*. 2011;117(8):2451-9.
54. Velichutina I, Shaknovich R, Geng HM, Johnson NA, Gascoyne RD, Melnick AM, et al. EZH2-mediated epigenetic silencing in germinal center B cells contributes to proliferation and lymphomagenesis. *Blood*. 2010;116(24):5247-55.
55. Davis RE, Brown KD, Siebenlist U, Staudt LM. Constitutive nuclear factor kappa B activity is required for survival of activated B cell-like diffuse large B cell lymphoma cells. *J Exp Med*. 2001;194(12):1861-74.
56. Baldwin AS. The NF-kappa B and I kappa B proteins: New discoveries and insights. *Annual Review of Immunology*. 1996;14:649-83.
57. Davis RE, Ngo VN, Lenz G, Tolar P, Young RM, Romesser PB, et al. Chronic active B-cell-receptor signalling in diffuse large B-cell lymphoma. *Nature*. 2010;463(7277):88-92.
58. Lenz G, Davis RE, Ngo VN, Lam L, George TC, Wright GW, et al. Oncogenic CARD11 mutations in human diffuse large B cell lymphoma. *Science*. 2008;319(5870):1676-9.

59. Compagno M, Lim WK, Grunn A, Nandula SV, Brahmachary M, Shen Q, et al. Mutations of multiple genes cause deregulation of NF-kappaB in diffuse large B-cell lymphoma. *Nature*. 2009;459(7247):717-21.
60. Ngo VN, Young RM, Schmitz R, Jhavar S, Xiao WM, Lim KH, et al. Oncogenically active MYD88 mutations in human lymphoma. *Nature*. 2011;470(7332):115-9.
61. Reth M, Hombach J, Wienands J, Campbell KS, Chien N, Justement LB, et al. The B-Cell Antigen Receptor Complex. *Immunol Today*. 1991;12(6):196-201.
62. Reth M. Antigen receptors on B lymphocytes. *Annu Rev Immunol*. 1992;10:97-121.
63. Reth M, Wienands J. Initiation and processing of signals from the B cell antigen receptor. *Annual Review of Immunology*. 1997;15:453-79.
64. Salamero J, Fougereau M, Seckinger P. Internalization of B-Cell and Pre-B-Cell Receptors Is Regulated by Tyrosine Kinase and Phosphatase-Activities. *Eur J Immunol*. 1995;25(10):2757-64.
65. Ma H, Yankee TM, Hu JJ, Asai DJ, Harrison ML, Geahlen RL. Visualization of Syk-antigen receptor interactions using green fluorescent protein: Differential roles for Syk and Lyn in the regulation of receptor capping and internalization. *J Immunol*. 2001;166(3):1507-16.
66. Staudt LM. Oncogenic Activation of NF-kappa B. *Csh Perspect Biol*. 2010;2(6).
67. McCully RR, Pomerantz JL. The protein kinase C-responsive inhibitory domain of CARD11 functions in NF-kappa B activation to regulate the association of multiple signaling cofactors that differentially depend on Bcl10 and MALT1 for association. *Mol Cell Biol*. 2008;28(18):5668-86.
68. Lamason RL, McCully RR, Lew SM, Pomerantz JL. Oncogenic CARD11 Mutations Induce Hyperactive Signaling by Disrupting Autoinhibition by the PKC-Responsive Inhibitory Domain. *Biochemistry-Us*. 2010;49(38):8240-50.
69. Akira S, Uematsu S, Takeuchi O. Pathogen recognition and innate immunity. *Cell*. 2006;124(4):783-801.

70. Wertz IE, O'Rourke KM, Zhou HL, Eby M, Aravind L, Seshagiri S, et al. De-ubiquitination and ubiquitin ligase domains of A20 downregulate NF-kappa B signalling. *Nature*. 2004;430(7000):694-9.
71. Stilo R, Varricchio E, Liguoro D, Leonardi A, Vito P. A20 is a negative regulator of BCL10- and CARMA3-mediated activation of NF-kappa B. *J Cell Sci*. 2008;121(8):1165-71.
72. Sun LJ, Deng L, Ea CK, Xia ZP, Chen ZJJ. The TRAF6 ubiquitin ligase and TAK1 kinase mediate IKK activation by BCL10 and MALT1 in T lymphocytes. *Mol Cell*. 2004;14(3):289-301.
73. Pasqualucci L, Compagno M, Houldsworth J, Monti S, Grunn A, Nandula SV, et al. Inactivation of the PRDM1/BLIMP1 gene in diffuse large B cell lymphoma. *J Exp Med*. 2006;203(2):311-7.
74. Shaffer AL, Lin KI, Kuo TC, Yu X, Hurt EM, Rosenwald A, et al. Blimp-1 orchestrates plasma cell differentiation by extinguishing the mature B cell gene expression program. *Immunity*. 2002;17(1):51-62.
75. Jones SE, Fuks Z, Kaplan HS, Rosenberg SA. Non-Hodgkins Lymphomas .5. Results of Radiotherapy. *Cancer*. 1973;32(3):682-91.
76. Jones SE, Kadin ME, Rosenber.Sa, Kaplan HS, Dorfman RF. Non-Hodgkins Lymphomas .2. Single Agent Chemotherapy. *Cancer*. 1972;30(1):31-8.
77. Fisher RI, Gaynor ER, Dahlberg S, Oken MM, Grogan TM, Mize EM, et al. Comparison of a standard regimen (CHOP) with three intensive chemotherapy regimens for advanced non-Hodgkin's lymphoma. *N Engl J Med*. 1993;328(14):1002-6.
78. Maloney DG, GrilloLopez AJ, Bodkin DJ, White CA, Liles TM, Royston I, et al. IDEC-C2B8: Results of a phase I multiple-dose trial in patients with relapsed non-Hodgkin's lymphoma. *J Clin Oncol*. 1997;15(10):3266-74.
79. Mohammed R, Milne A, Kayani K, Ojha U. How the discovery of rituximab impacted the treatment of B-cell non-Hodgkin's lymphomas. *J Blood Med*. 2019;10:71-84.

80. Korkolopoulou P, Vassilakopoulos T, Milionis V, Ioannou M. Recent Advances in Aggressive Large B-cell Lymphomas: A Comprehensive Review. *Adv Anat Pathol.* 2016;23(4):202-43.
81. Xue F, Cooley L. kelch encodes a component of intercellular bridges in *Drosophila* egg chambers. *Cell.* 1993;72(5):681-93.
82. Robinson DN, Cant K, Cooley L. Morphogenesis of *Drosophila* Ovarian Ring Canals. *Development.* 1994;120(7):2015-25.
83. Schupbach T, Wieschaus E. Female Sterile Mutations on the 2nd Chromosome of *Drosophila-Melanogaster* .2. Mutations Blocking Oogenesis or Altering Egg Morphology. *Genetics.* 1991;129(4):1119-36.
84. Adams J, Kelso R, Cooley L. The kelch repeat superfamily of proteins: propellers of cell function. *Trends Cell Biol.* 2000;10(1):17-24.
85. Prag S, Adams JC. Molecular phylogeny of the kelch-repeat superfamily reveals an expansion of BTB/kelch proteins in animals. *Bmc Bioinformatics.* 2003;4.
86. Varghese JN, Laver WG, Colman PM. Structure of the Influenza-Virus Glycoprotein Antigen Neuraminidase at 2.9-Å Resolution. *Nature.* 1983;303(5912):35-40.
87. Bork P, Doolittle RF. *Drosophila* Kelch Motif Is Derived from a Common Enzyme Fold. *J Mol Biol.* 1994;236(5):1277-82.
88. Bardwell VJ, Treisman R. The Poz Domain - a Conserved Protein-Protein Interaction Motif. *Gene Dev.* 1994;8(14):1664-77.
89. Ahmad KF, Engel CK, Prive GG. Crystal structure of the BTB domain from PLZF. *P Natl Acad Sci USA.* 1998;95(21):12123-8.
90. Li XC, Zhang D, Hannink M, Beamer LJ. Crystal structure of the Kelch domain of human Keap1. *J Biol Chem.* 2004;279(52):54750-8.

91. Tseng LA, Bixby JL. Interaction of an intracellular pentraxin with a BTB-Kelch protein is associated with ubiquitylation, aggregation and neuronal apoptosis. *Mol Cell Neurosci.* 2011;47(4):254-64.
92. Canning P, Cooper CDO, Krojer T, Murray JW, Pike ACW, Chaikuad A, et al. Structural Basis for Cul3 Protein Assembly with the BTB-Kelch Family of E3 Ubiquitin Ligases. *J Biol Chem.* 2013;288(11):7803-14.
93. Kobayashi A, Kang MI, Okawa H, Ohtsuji M, Zenke Y, Chiba T, et al. Oxidative stress sensor Keap1 functions as an adaptor for Cul3-based E3 ligase to regulate for proteasomal degradation of Nrf2. *Mol Cell Biol.* 2004;24(16):7130-9.
94. Liu CC, Lin YC, Chen YH, Chen CM, Pang LY, Chen HA, et al. Cul3-KLHL20 Ubiquitin Ligase Governs the Turnover of ULK1 and VPS34 Complexes to Control Autophagy Termination. *Mol Cell.* 2016;61(1):84-97.
95. Petroski MD, Deshaies RJ. Function and regulation of Cullin-RING ubiquitin ligases. *Nat Rev Mol Cell Bio.* 2005;6(1):9-20.
96. Dhanoa BS, Cogliati T, Satish AG, Bruford EA, Friedman JS. Update on the Kelch-like (KLHL) gene family. *Hum Genomics.* 2013;7.
97. Pintard L, Willems A, Peter M. Cullin-based ubiquitin ligases: Cul3-BTB complexes join the family. *Embo J.* 2004;23(8):1681-7.
98. Gupta-Rossi N, Storck S, Griebel PJ, Reynaud CA, Weill JC, Dahan A. Specific over-expression of deltex and a new Kelch-like protein in human germinal center B cells. *Mol Immunol.* 2003;39(13):791-9.
99. Kroll J, Shi XZ, Caprioli A, Liu HH, Waskow C, Lin KM, et al. The BTB-kelch protein KLHL6 is involved in B-lymphocyte antigen receptor signaling and germinal center formation. *Mol Cell Biol.* 2005;25(19):8531-40.
100. Stogios PJ, Prive GG. The BACK domain in BTB-kelch proteins. *Trends Biochem Sci.* 2004;29(12):634-7.

101. Bertocci B, Lecoeuche D, Sterlin D, Kuhn J, Gaillard B, De Smet A, et al. Klhl6 Deficiency Impairs Transitional B Cell Survival and Differentiation. *J Immunol*. 2017;199(7):2408-20.
102. Puente XS, Pinyol M, Quesada V, Conde L, Ordonez GR, Villamor N, et al. Whole-genome sequencing identifies recurrent mutations in chronic lymphocytic leukaemia. *Nature*. 2011;475(7354):101-5.
103. Kim JA, Hwang B, Park SN, Huh S, Im K, Choi S, et al. Genomic Profile of Chronic Lymphocytic Leukemia in Korea Identified by Targeted Sequencing. *Plos One*. 2016;11(12).
104. Ganapathi KA, Jobanputra V, Iwamoto F, Jain P, Chen JL, Cascione L, et al. The genetic landscape of dural marginal zone lymphomas. *Oncotarget*. 2016;7(28):43052-61.
105. Weigert O, Kopp N, Lane AA, Yoda A, Dahlberg SE, Neuberg D, et al. Molecular Ontogeny of Donor-Derived Follicular Lymphomas Occurring after Hematopoietic Cell Transplantation. *Cancer Discov*. 2012;2(1):47-55.
106. Luthra R, Patel KP, Reddy NG, Haghshenas V, Routbort MJ, Harmon MA, et al. Next-generation sequencing-based multigene mutational screening for acute myeloid leukemia using MiSeq: applicability for diagnostics and disease monitoring. *Haematologica*. 2014;99(3):465-73.
107. Chapuy B, Stewart C, Dunford AJ, Kim J, Kamburov A, Redd RA, et al. Molecular subtypes of diffuse large B cell lymphoma are associated with distinct pathogenic mechanisms and outcomes. *Nat Med*. 2018;24(5):679-90.
108. Lohr JG, Stojanov P, Lawrence MS, Auclair D, Chapuy B, Sougnez C, et al. Discovery and prioritization of somatic mutations in diffuse large B-cell lymphoma (DLBCL) by whole-exome sequencing. *P Natl Acad Sci USA*. 2012;109(10):3879-84.
109. Reddy A, Zhang J, Davis NS, Moffitt AB, Love CL, Waldrop A, et al. Genetic and Functional Drivers of Diffuse Large B Cell Lymphoma. *Cell*. 2017;171(2):481-94.
110. Mareschal S, Pham-Ledard A, Viailly PJ, Dubois S, Bertrand P, Maingonnat C, et al. Identification of Somatic Mutations in Primary Cutaneous Diffuse Large B-Cell Lymphoma, Leg Type by Massive Parallel Sequencing. *J Invest Dermatol*. 2017;137(9):1984-94.

111. Fallahi-Sichani M, Honarnejad S, Heiser LM, Gray JW, Sorger PK. Metrics other than potency reveal systematic variation in responses to cancer drugs. *Nat Chem Biol.* 2013;9(11):708-14.
112. Yadav B, Pemovska T, Szwajda A, Kuleskiy E, Kontro M, Karjalainen R, et al. Quantitative scoring of differential drug sensitivity for individually optimized anticancer therapies. *Sci Rep-Uk.* 2014;4.
113. Hecht BK, Epstein AL, Berger CS, Kaplan HS, Hecht F. Histiocytic lymphoma cell lines: immunologic and cytogenetic studies. *Cancer Genet Cytogenet.* 1985;14(3-4):205-18.
114. DSMZ - German Collection of Microorganisms and Cell Cultures. SU-DHL-4 (ACC 495) 2019 [cited 2019 10th September]. Available from: <https://www.dsmz.de/collection/catalogue/details/culture/ACC-495>.
115. DSMZ - German Collection of Microorganisms and Cell Cultures. SU-DHL-5 (ACC 571) 2019 [cited 2019 18th June]. Available from: <https://www.dsmz.de/catalogues/details/culture/ACC-571.html>.
116. Root D. pLEX_307: David Root Lab Plasmids; 2012 [cited 2019 16th August]. Available from: <https://www.addgene.org/41392/>.
117. Tandaric L. DSRT Pipeline - Raw Data and Supplementary Material. Helsinki, Finland: University of Helsinki; 2019 [2019]. Available from: <https://breeze.fimm.fi/DSRT/dWwvLEyGGtTPW0502Rrqnplrqhkmla3QBdd2yBs/Results/HTMLreport/qc.html>.
118. International Cell Line Authentication Committee. Guide to Human Cell Line Authentication 2014 [cited 2019 21st June]. Available from: <https://iclac.org/resources/human-cell-line-authentication/>.
119. Pemovska T, Kontro M, Yadav B, Edgren H, Eldfors S, Szwajda A, et al. Individualized Systems Medicine Strategy to Tailor Treatments for Patients with Chemorefractory Acute Myeloid Leukemia. *Cancer Discov.* 2013;3(12):1416-29.

120. Pemovska T, Johnson E, Kontro M, Repasky GA, Chen J, Wells P, et al. Axitinib effectively inhibits BCR-ABL1(T315I) with a distinct binding conformation. *Nature*. 2015;519(7541):102-5.
121. Pietarinen PO, Pemovska T, Kontro M, Yadav B, Mpindi JP, Andersson EI, et al. Novel drug candidates for blast phase chronic myeloid leukemia from high-throughput drug sensitivity and resistance testing. *Blood Cancer J*. 2015;5.
122. Majumder MM, Silvennoinen R, Anttila P, Tamborero D, Eldfors S, Yadav B, et al. Identification of precision treatment strategies for relapsed/refractory multiple myeloma by functional drug sensitivity testing. *Oncotarget*. 2017;8(34):56338-50.
123. Dufva O, Kankainen M, Kelkka T, Sekiguchi N, Awad SA, Eldfors S, et al. Aggressive natural killer-cell leukemia mutational landscape and drug profiling highlight JAK-STAT signaling as therapeutic target. *Nat Commun*. 2018;9.

8. CURRICULUM VITAE

Personal Information:

Name and Surname: Luka Tandarić

Born: 21st November 1995 in Osijek, Croatia

Education:

02.10.2017 - Today : Master's Program in Molecular Biology (MSc.) -
University of Zagreb - Faculty of Science - Dept. of Biology

29.09.2014 - 04.09.2017 : Bachelor's Program in Molecular Biology (BSc.) -
University of Zagreb - Faculty of Science - Dept. of Biology

Work Experience and Training:

01.03.2019 - 01.09.2019 : Erasmus+ SMP / Research Assistant Position - Lymphoma
Biology and Survival Group - Research Programs Unit - Faculty of Medicine -
University of Helsinki

01.08.2018 - 01.10.2018 : Erasmus+ SMP - Lymphoma Biology and Survival Group
- Research Programs Unit - Faculty of Medicine - University of Helsinki

26.02.2018 - 15.06.2018 : Molecular Biology Laboratory Skill Training (Elective
Course) - University of Zagreb - Faculty of Science - Dept. of Biology -
Division of Molecular Biology

Skills:

English (C1)

Proficient in digital skills

Category B driver's license